EUROPEAN ORGANIZATION FOR NUCLEAR RESEARCH

CERN-PPE/91-186
4 November 1991

Measurement of Tau Branching Ratios

The ALEPH Collaboration*

Abstract

Using the data accumulated at LEP in 1989 and 1990 with the ALEPH detector, the inclusive and exclusive branching ratios of the τ lepton have been measured assuming lepton universality in Z^0 decays. The inclusive branching fractions for the τ decay into one, three, and five charged particles have been determined to be $(85.45 \pm 0.97)\%$, $(14.35 \pm 0.48)\%$, and $(0.10 \pm 0.05)\%$, respectively, in agreement with the world averages. New undetected decay modes are determined to have a branching fraction of less than 2.1% at 95% CL. The measured branching ratios for quasi–exclusive channels are slightly larger than, but consistent with the world averages, except for the modes $\tau \to 3\,\text{hadrons} + \nu_\tau$ and $\tau \to \text{hadron} + 2\pi^0\nu_\tau$, which are significantly larger. These latter branching ratios have been found to be $(9.5 \pm 0.7)\%$ and $(10.2 \pm 1.1)\%$, respectively. The sum of all the measured quasi–exclusive branching ratios is $(100.4 \pm 1.8)\%$. A fully exclusive analysis of modes with neutral pions shows no evidence for new photonic decay modes with a branching fraction limit of 3.4% at 95% CL.

(Submitted to *Zeitschrift für Physik* C)

* See the following pages for the list of authors

The ALEPH Collaboration

D. Decamp, B. Deschizeaux, C. Goy, J.-P. Lees, M.-N. Minard

Laboratoire de Physique des Particules (LAPP), IN^{2}P^3-CNRS, 74019 Annecy-le-Vieux Cedex, France

R. Alemany, J.M. Crespo, M. Delfino, E. Fernandez, V. Gaitan, Ll. Garrido, Ll.M. Mir, A. Pacheco

Laboratorio de Fisica de Altas Energias, Universidad Autonoma de Barcelona, 08193 Bellaterra (Barcelona), Spain[8]

M.G. Catanesi, D. Creanza, M. de Palma, A. Farilla, G. Iaselli, G. Maggi, M. Maggi, S. Natali, S. Nuzzo, M. Quattromini, A. Ranieri, G. Raso, F. Romano, F. Ruggieri, G. Selvaggi, L. Silvestris, P. Tempesta, G. Zito

INFN Sezione di Bari e Dipartimento di Fisica dell' Università, 70126 Bari, Italy

Y. Gao, H. Hu,[21] D. Huang, X. Huang, J. Lin, J. Lou, C. Qiao,[21] T. Ruan,[21] T. Wang, Y. Xie, D. Xu, R. Xu, J. Zhang, W. Zhao

Institute of High-Energy Physics, Academia Sinica, Beijing, The People's Republic of China[9]

W.B. Atwood,[2] L.A.T. Bauerdick, F. Bird,[4] E. Blucher, G. Bonvicini, F. Bossi, J. Boudreau, T.H. Burnett,[3] H. Drevermann, R.W. Forty, C. Grab,[23] R. Hagelberg, S. Haywood, J. Hilgart, B. Jost, M. Kasemann,[28] J. Knobloch, A. Lacourt, E. Lançon, I. Lehraus, T. Lohse, A. Lusiani, A. Marchioro, M. Martinez, P. Mato, S. Menary,[29] T. Meyer, A. Minten, A. Miotto, R. Miquel, H.-G. Moser, J. Nash, P. Palazzi, F. Ranjard, G. Redlinger, L. Rolandi,[30] A. Roth,[32] J. Rothberg,[3] M. Saich, D. Schlatter, M. Schmelling, W. Tejessy, H. Wachsmuth, S. Wasserbaech, W. Wiedenmann, W. Witzeling, J. Wotschack

European Laboratory for Particle Physics (CERN), 1211 Geneva 23, Switzerland

Z. Ajaltouni, F. Badaud, M. Bardadin-Otwinowska, A.M. Bencheikh, R. El Fellous, A. Falvard, P. Gay, C. Guicheney, P. Henrard, J. Jousset, B. Michel, J-C. Montret, D. Pallin, P. Perret, B. Pietrzyk, J. Proriol, F. Prulhière, G. Stimpfl

Laboratoire de Physique Corpusculaire, Université Blaise Pascal, IN^{2}P^3-CNRS, Clermont-Ferrand, 63177 Aubière, France

J.D. Hansen, J.R. Hansen, P.H. Hansen, R. Møllerud, B.S. Nilsson

Niels Bohr Institute, 2100 Copenhagen, Denmark[10]

I. Efthymiopoulos, E. Simopoulou, A. Vayaki

Nuclear Research Center Demokritos (NRCD), Athens, Greece

J. Badier, A. Blondel, G. Bonneaud, J.C. Brient, G. Fouque, A. Gamess, J. Harvey, S. Orteu, A. Rosowsky, A. Rougé, M. Rumpf, R. Tanaka, H. Videau

Laboratoire de Physique Nucléaire et des Hautes Energies, Ecole Polytechnique, IN^{2}P^3-CNRS, 91128 Palaiseau Cedex, France

D.J. Candlin, E. Veitch

Department of Physics, University of Edinburgh, Edinburgh EH9 3JZ, United Kingdom[11]

L. Moneta, G. Parrini

Dipartimento di Fisica, Università di Firenze, INFN Sezione di Firenze, 50125 Firenze, Italy

M. Corden, C. Georgiopoulos, M. Ikeda, J. Lannutti, D. Levinthal,[16] M. Mermikides, L. Sawyer

Supercomputer Computations Research Institute and Dept. of Physics, Florida State University, Tallahassee, FL 32306, USA [13,14,15]

A. Antonelli, R. Baldini, G. Bencivenni, G. Bologna,[5] P. Campana, G. Capon, F. Cerutti, V. Chiarella, B. D'Ettorre-Piazzoli,[34] G. Felici, P. Laurelli, G. Mannocchi,[6] F. Murtas, G.P. Murtas, L. Passalacqua, M. Pepe-Altarelli, P. Picchi,[5] P. Zografou

Laboratori Nazionali dell'INFN (LNF-INFN), 00044 Frascati, Italy

B. Altoon, O. Boyle, P. Colrain, A.W. Halley, I. ten Have, J.G. Lynch, W. Maitland, W.T. Morton, C. Raine, J.M. Scarr, K. Smith, A.S. Thompson, R.M. Turnbull

Department of Physics and Astronomy, University of Glasgow, Glasgow G12 8QQ, United Kingdom[11]

B. Brandl, O. Braun, R. Geiges, C. Geweniger, P. Hanke, V. Hepp, E.E. Kluge, Y. Maumary, A. Putzer, B. Rensch, A. Stahl, K. Tittel, M. Wunsch

Institut für Hochenergiephysik, Universität Heidelberg, 6900 Heidelberg, Fed. Rep. of Germany[17]

A.T. Belk, R. Beuselinck, D.M. Binnie, W. Cameron, M. Cattaneo, P.J. Dornan,[1] S. Dugeay, A.M. Greene, J.F. Hassard, N.M. Lieske, S.J. Patton, D.G. Payne, M.J. Phillips, J.K. Sedgbeer, G. Taylor, I.R. Tomalin, A.G. Wright

Department of Physics, Imperial College, London SW7 2BZ, United Kingdom[11]

P. Girtler, D. Kuhn, G. Rudolph

Institut für Experimentalphysik, Universität Innsbruck, 6020 Innsbruck, Austria[19]

C.K. Bowdery, T.J. Brodbeck, A.J. Finch, F. Foster, G. Hughes, D. Jackson, N.R. Keemer, M. Nuttall, A. Patel, T. Sloan, S.W. Snow, E.P. Whelan

Department of Physics, University of Lancaster, Lancaster LA1 4YB, United Kingdom[11]

T. Barczewski, K. Kleinknecht, J. Raab, B. Renk, S. Roehn, H.-G. Sander, H. Schmidt, F. Steeg, S.M. Walther, B. Wolf

Institut für Physik, Universität Mainz, 6500 Mainz, Fed. Rep. of Germany[17]

J-J. Aubert, C. Benchouk, V. Bernard, A. Bonissent, J. Carr, P. Coyle, J. Drinkard, F. Etienne, S. Papalexiou, P. Payre, Z. Qian, D. Rousseau, P. Schwemling, M. Talby

Centre de Physique des Particules, Faculté des Sciences de Luminy, IN²P³-CNRS, 13288 Marseille, France

S. Adlung, H. Becker, W. Blum, D. Brown, P. Cattaneo,[31] G. Cowan, B. Dehning, H. Dietl, F. Dydak,[26] M. Fernandez-Bosman, T. Hansl-Kozanecka,[2,22] A. Jahn, W. Kozanecki,[2] E. Lange, J. Lauber, G. Lütjens, G. Lutz, W. Männer, Y. Pan, R. Richter, H. Rotscheidt, J. Schröder, A.S. Schwarz, R. Settles, U. Stierlin, U. Stiegler, R. St. Denis, M. Takashima, J. Thomas,[4] G. Wolf

Max-Planck-Institut für Physik und Astrophysik, Werner-Heisenberg-Institut für Physik, 8000 München, Fed. Rep. of Germany[17]

V. Bertin, J. Boucrot, O. Callot, X. Chen, A. Cordier, M. Davier, J.-F. Grivaz, Ph. Heusse, P. Janot, D.W. Kim,[20] F. Le Diberder, J. Lefrançois,[1] A.-M. Lutz, M.-H. Schune, J.-J. Veillet, I. Videau, Z. Zhang, F. Zomer

Laboratoire de l'Accélérateur Linéaire, Université de Paris-Sud, IN²P³-CNRS, 91405 Orsay Cedex, France

D. Abbaneo, S.R. Amendolia, G. Bagliesi, G. Batignani, L. Bosisio, U. Bottigli, C. Bradaschia, M. Carpinelli, M.A. Ciocci, R. Dell'Orso, I. Ferrante, F. Fidecaro,[1] L. Foà, E. Focardi, F. Forti, C. Gatto, A. Giassi, M.A. Giorgi, F. Ligabue, E.B. Mannelli, P.S. Marrocchesi, A. Messineo, F. Palla, G. Sanguinetti, J. Steinberger, R. Tenchini, G. Tonelli, G. Triggiani, C. Vannini, A. Venturi, P.G. Verdini, J. Walsh

Dipartimento di Fisica dell'Università, INFN Sezione di Pisa, e Scuola Normale Superiore, 56010 Pisa, Italy

J.M. Carter, M.G. Green, P.V. March, T. Medcalf, I.S. Quazi, J.A. Strong, L.R. West, T. Wildish

Department of Physics, Royal Holloway & Bedford New College, University of London, Surrey TW20 OEX, United Kingdom[11]

D.R. Botterill, R.W. Clifft, T.R. Edgecock, M. Edwards, S.M. Fisher, T.J. Jones, P.R. Norton, D.P. Salmon, J.C. Thompson

Particle Physics Dept., Rutherford Appleton Laboratory, Chilton, Didcot, Oxon OX11 OQX, United Kingdom[11]

B. Bloch-Devaux, P. Colas, E. Locci, S. Loucatos, E. Monnier, P. Perez, J.A. Perlas, F. Perrier, J. Rander, J.-F. Renardy, A. Roussarie, J.-P. Schuller, J. Schwindling, B. Vallage

Département de Physique des Particules Elémentaires, CEN-Saclay, 91191 Gif-sur-Yvette Cedex, France[18]

J.G. Ashman, C.N. Booth, C. Buttar, R.E. Carney, S. Cartwright, F. Combley, M. Dogru, F. Hatfield, J. Martin, D. Parker, P. Reeves, L.F. Thompson

Department of Physics, University of Sheffield, Sheffield S3 7RH, United Kingdom[11]

E. Barberio, S. Brandt, C. Grupen, H. Meinhard, L. Mirabito,[33] U. Schäfer, H. Seywerd

Fachbereich Physik, Universität Siegen, 5900 Siegen, Fed. Rep. of Germany[17]

G. Ganis, G. Giannini, B. Gobbo, F. Ragusa,[25]

Dipartimento di Fisica, Università di Trieste e INFN Sezione di Trieste, 34127 Trieste, Italy

L. Bellantoni, D. Cinabro, J.S. Conway, D.F. Cowen,[24] Z. Feng, D.P.S. Ferguson, Y.S. Gao, J. Grahl, J.L. Harton, R.C. Jared,[7] R.P. Johnson,[27] B.W. LeClaire, C. Lishka, Y.B. Pan, J.R. Pater, Y. Saadi, V. Sharma, Z.H. Shi, Y.H. Tang, A.M. Walsh, J.A. Wear,[27] F.V. Weber, M.H. Whitney, Sau Lan Wu, G. Zobernig

Department of Physics, University of Wisconsin, Madison, WI 53706, USA[12]

[1] Now at CERN, PPE Division, 1211 Geneva 23, Switzerland.
[2] Permanent adddress: SLAC, Stanford, CA 94309, USA.
[3] Permanent address: University of Washington, Seattle, WA 98195, USA.
[4] Now at SSCL, Dallas, TX, U.S.A.
[5] Also Istituto di Fisica Generale, Università di Torino, Torino, Italy.
[6] Also Istituto di Cosmo-Geofisica del C.N.R., Torino, Italy.
[7] Permanent address: LBL, Berkeley, CA 94720, USA.
[8] Supported by CAICYT, Spain.
[9] Supported by the National Science Foundation of China.
[10] Supported by the Danish Natural Science Research Council.
[11] Supported by the UK Science and Engineering Research Council.
[12] Supported by the US Department of Energy, contract DE-AC02-76ER00881.
[13] Supported by the US Department of Energy, contract DE-FG05-87ER40319.
[14] Supported by the NSF, contract PHY-8451274.
[15] Supported by the US Department of Energy, contract DE-FC0S-85ER250000.
[16] Supported by SLOAN fellowship, contract BR 2703.
[17] Supported by the Bundesministerium für Forschung und Technologie, Fed. Rep. of Germany.
[18] Supported by the Institut de Recherche Fondamentale du C.E.A.
[19] Supported by Fonds sur Förderung der wissenschaftlichen Forschung, Austria.
[20] Supported by the Korean Science and Engineering Foundation and Ministry of Education.
[21] Supported by the World Laboratory.
[22] On leave of absence from MIT, Cambridge, MA 02139, USA.
[23] Now at ETH, Zürich, Switzerland.
[24] Now at California Institute of Technology, Pasadena, CA 91125, USA.
[25] Now at Dipartimento di Fisica, Università di Milano, Milano, Italy.
[26] Also at CERN, PPE Division, 1211 Geneva 23, Switzerland.
[27] Now at University of California, Santa Cruz, CA 95064, USA.
[28] Now at DESY, Hamburg, Germany.
[29] Now at Cornell University, Ithaca, NY 14853, USA.
[30] Also at Dipartimento di Fisica, Università di Trieste, Trieste, Italy.
[31] Now at INFN, Pavia, Italy.
[32] Now at Lufthansa, Hamburg, Germany.
[33] Now at Institut de Physique Nucléaire de Lyon, 69622 Villeurbanne, France.
[34] Also at Università di Napoli, Dipartimento di Scienze Fisiche, Napoli, Italy.

1 Introduction

The experimental situation on the τ branching fractions is uncertain in that there exist several discrepancies among different investigations[1]. In particular the so–called "one–prong problem"[2,3] has been a long–standing puzzle: measurements of single channels by different experiments lead to a deficit in the sum of the branching ratios B_i for exclusive one–prong channels compared to the corresponding one–prong inclusive fraction(B_1^T). Using the latest world–average values, this deficit amounts to[4]

$$\Delta B_{\rm WA} = B_1^T - \sum_i B_i(\text{one–prong}) = +(4.2 \pm 3.1)\% \; . \tag{1}$$

A larger discrepancy is obtained by using for the channel $\tau \to \pi 3\pi^0 \nu_\tau$ the theoretical prediction[3,5,6] based on CVC and e^+e^- data instead of the imprecise experimental value, with the result

$$\Delta B_{\rm WA} = +(5.8 \pm 1.4)\% \; . \tag{2}$$

Whether the quoted effect in Eq.(2) is the result of uncontrolled systematic effects between experiments or a signal for undetected decay modes of the τ lepton is largely an open matter. A possible solution has been indicated by the CELLO experiment[7] in a global analysis of the τ branching fractions, which yielded larger branching ratios for the $\tau \to 3\pi\nu_\tau$ and $\pi 2\pi^0 \nu_\tau$ modes than those determined previously.

In this paper a global analysis of the τ branching ratios is presented using a clean sample of τ leptons from Z^0 decays at LEP and taking into account the particularly advantageous properties of the ALEPH detector for this investigation and the feasibility of an accurate absolute normalization for the $\tau^+\tau^-$ sample on the basis of the other leptons. The latter allows the measurement of absolute branching ratios for all detected τ–decay channels and, therefore, opens the possibility to search for "missing" decays.

This analysis is performed to investigate the following aspects:

- The inclusive measurement of topological (charged prong) branching ratios: the analysis is applied to complete $\tau^+\tau^-$ events with respect to their global topology. A sum of branching ratios less than 100% would indicate the existence of τ decays which are not selected by the analysis.

- The measurement of quasi–exclusive branching ratios for all channels: in this case, further cuts are required for particle identification and the basic sample consists of all identified τ decay candidates. Here τ decays are classified in generic classes defined by the number of charged particles, the number of reconstructed π^0's, and the photon multiplicity to take into account single or unresolved photons originating from π^0 decays and possibly from other sources.

- The measurement of exclusive branching ratios: exclusive modes are defined on the basis of reconstructed π^0's only. The corresponding branching ratios are compared with the results of the quasi–exclusive analysis to set a limit on the existence of possible channels where photons may not come exclusively from π^0 decays, for example decays involving η's.

Emphasis is placed on redundancy and control of possible systematic effects. The description of the ALEPH detector, the event selection, particle identification, γ/π^0 reconstruction, the Monte Carlo generator for τ production and decays, and the different analysis methods and their results are presented in turn.

2 The ALEPH Detector

A detailed description of the ALEPH detector can be found in Ref.[8]. Despite the fact that, at LEP energies, τ decays are collimated in a cone of a few degrees opening angle, ALEPH is well suited to study these decays because of its excellent granularity in the different subdetectors.

The primary ALEPH tracking device is a large time projection chamber (TPC) providing three–dimensional track coordinates with the following properties: large radial coverage (from 0.3 to 1.8 m), accurate spatial precision (160 μm for the $r\phi$ coordinate transverse to the beam axis, 1 mm for the z coordinate along the beam axis), and a large number of space coordinates along a track (up to 21). Inside the TPC, an inner tracking chamber (ITC) provides $r\phi$ coordinates for tracking and triggering. In the presence of a 1.5 Tesla magnetic field, the two subdetectors provide[9] a transverse momentum resolution of:

$$\frac{\Delta p_T}{p_T} = 8 \times 10^{-4} p_T \ (\mathrm{GeV/c}) \ , \tag{3}$$

and an angular separation between two tracks of less than 1°.

A finely segmented electromagnetic calorimeter (ECAL), consisting of 45 layers of lead interleaved with proportional tubes, is located inside the superconducting coil to minimize the amount of intervening material. It is built in 36 modules, twelve in the barrel part and twelve in each endcap. Cathode pads in each layer are connected internally to form "towers" pointing towards the interaction point. Each of the 77,728 towers, covering an angular width of typically $0.9° \times 0.9°$, is read–out in three sections ("stacks") of 4, 9, and 9 radiation lengths in depth. A shower is spread over several towers ("cluster") and its centroid is measured with an accuracy of 2 mm. The energy resolution is

$$\frac{\Delta E}{E} = 0.017 + \frac{0.19}{\sqrt{E(\mathrm{GeV})}} \ . \tag{4}$$

The hadron calorimeter (HCAL) has 23 layers of iron absorber each 5 cm thick with limited streamer tubes 9×9 mm^2 in cross section between each layer. The tower read–out is built from pads with an angular size of $3.7° \times 3.7°$. Strips running along the tubes provide a digital read–out giving a two–dimensional view of the development of hadronic showers and muon trajectories. The two calorimeters, ECAL and HCAL, are rotated by 2° with respect to each other to avoid overlapping of the small gaps ("cracks") between modules.

Particle identification is achieved using dE/dx in the TPC (up to 360 samplings, of which the lowest 60% are used to calculate a truncated mean), the energy deposits in the three stacks of ECAL, and the shower pattern in HCAL.

Events are recorded in ALEPH if they satisfy a three–level triggering procedure. The main first level triggers are:

- ECAL energy greater than 6.5 GeV in the barrel or 3.8 GeV in either endcap or greater than 1.6 GeV in both endcaps.
- ECAL energy greater than 1.3 GeV (reduced to 0.2 GeV in the data of 1990) in a module in the same azimuthal region as an ITC track.
- A particle penetrating HCAL in the same azimuthal region as an ITC track.

A number of subsidiary triggers provide redundancy and allow the trigger efficiencies to be studied. The trigger inefficiency is 0.15% for $\tau^+\tau^-$ events within the fiducial region and is known with an accuracy better than 0.05%.

3 Event Selection

This analysis has been performed on data collected by ALEPH in 1989 and 1990 in a scan of the Z^0 peak. About 50% of the integrated luminosity was taken at the peak (91.2 GeV), the remainder being distributed over six energies spaced at 1 GeV intervals across the resonance.

To isolate $\tau^+\tau^-$ events, essentially the same criteria are used as for the measurement of the total cross section and the forward–backward asymmetry in the $e^+e^- \rightarrow \tau^+\tau^-$ process[10], with some improvements aimed at reducing the hadronic background. The following requirements are designed to reject events from $Z^0 \rightarrow e^+e^-(\gamma)$, $\mu^+\mu^-(\gamma)$, and $q\bar{q}(g)$, and from $\gamma\gamma$–induced processes:

1. A track must have at least four space points in the TPC and originate from the beam crossing point to within 5 cm along the beam axis and 2 cm in the transverse direction.
2. The event is required to have two to six tracks in the polar angle range $|\cos\theta| < 0.95$.
3. The event, divided into two hemispheres by a plane perpendicular to the thrust axis, must have at least one track in each hemisphere.
4. At least one track must have a reconstructed momentum greater than 3 GeV/c.
5. The track momenta in each hemisphere are summed vectorially. The acollinearity η, defined as 180° minus the angle between these vector sums, has to be smaller than 20°.

6. The transverse momentum relative to the beam axis of the vector sum of the tracks in each hemisphere must be larger than 2.5 GeV/c in at least one of the two hemispheres.

7. Events with more than 4 tracks are rejected if any track makes an angle greater than 18.2° with the vector sum of the track momenta in the same hemisphere.

8. The square of the missing mass calculated from the tracks (assuming pion masses) and the initial state (with energy $\sqrt{s}$) is required to exceed $400\, s/M_Z^2$ $(\mathrm{GeV/c^2})^2$.

9. The measured energy in ECAL must be less than $55\sqrt{s}/M_Z$ GeV.

10. Events are rejected if both hemispheres have a mass larger than 3 $\mathrm{GeV/c^2}$, the mass being computed with charged particles, photons and neutral hadrons, as determined by an energy flow procedure[11].

11. If $\theta_\pm$ are the polar angles of the momentum vector sums in each hemisphere, the polar angle of the $\tau^+\tau^-$ pair in its centre of mass is approximately given by

$$\cos\theta^* = \frac{\sin\left(\frac{\theta_+ - \theta_-}{2}\right)}{\sin\left(\frac{\theta_+ + \theta_-}{2}\right)}\ , \tag{5}$$

and is required to satisfy

$$|\cos\theta^*| < 0.90\ . \tag{6}$$

The vertex constraint (1) eliminates most tracks which originate from beam–gas interactions, cosmic rays, and badly measured events. The multiplicity cut (2), the collimation cut (7) and the mass cut (10) remove hadronic Z^0 decays. Two–photon interactions are rejected with cuts (3), (4), (5), and (6). Finally, $e^+e^-(\gamma)$ and $\mu^+\mu^-(\gamma)$ events are removed by cuts (8) and (9).

The selection procedure has an overall efficiency of $(72.4 \pm 0.8)\%$ corresponding to a selection efficiency of 84.5% within the geometric acceptance given by cut (11). The systematic error stems mostly from the ECAL wire energy and missing–mass cuts and was determined directly on the data in Refs.[10] and [12].

The background contaminations are estimated from Monte Carlo simulations to be $(1.1 \pm 0.5)\%$ from $Z \to e^+e^-$, $(0.17 \pm 0.08)\%$ from $Z \to \mu^+\mu^-$, and $(0.24 \pm 0.06)\%$ from $Z \to q\bar{q}$. The background from $\gamma\gamma \to e^+e^-$, $\mu^+\mu^-$, and $\tau^+\tau^-$ are estimated to be (4.5 ± 0.9), (4.7 ± 0.7), and (0.8 ± 0.1) pb, respectively. The background from $\gamma\gamma \to q\bar{q}$ and cosmic rays is found to be negligible. These different background estimates have been checked on the selected data by enlarging the cuts or by looking at restricted event samples which are more sensitive to the background level than the selected sample. Some indication of an overestimate of the $\gamma\gamma$ contamination is observed and a correction of (0.85 ± 0.15) has been applied to the Monte Carlo estimate. The other background sources are found to be correctly described by the Monte Carlo simulation. Integrating the data across the Z^0 resonance, the overall background contamination amounts to 2.4%.

Periods of data taking where detectors or data acquisition were showing signs of misbehaviour were excluded from the data sample. In addition, some individual ECAL or HCAL modules occasionally experienced coherent noise pick–up or amplifier problems. In such cases, it was required that the thrust axis of the event did not point to the bad module with a tolerance of typically 20° around it in order to be safe for photon reconstruction and/or particle identification. The inefficiency introduced by this procedure (5.6% and 6.7% for the inclusive and exclusive analyses, respectively) has been directly determined from the data.

4 Particle Identification

4.1 The method

Particle identification is crucial for the measurement of the τ branching ratios. Two cases are particularly important: (i) electron identification where electrons or positrons from photon conversions are searched for in order to restore the original charged particle topology in the inclusive analysis, and to reconstruct the corresponding photons in the exclusive analysis; and (ii) general particle identification where electrons, muons, and hadrons have to be distinguished one from the other in order to classify one–prong τ decays.

Electron identification is based on dE/dx in the TPC and on two variables which measure the degree to which an energy deposit in the ECAL towers near an extrapolated track conforms to that expected from an electron. The first variable, R_T, compares the measured momentum p to the energy E deposited in the four towers closest to the extrapolated track. Test beam data have shown that the variable $x = \frac{E}{p}$ has a Gaussian distribution for electrons with a mean $\overline{x}$ and a variance σ^2. Then

$$R_T = \frac{x - \overline{x}}{\sigma} \tag{7}$$

is normally distributed with a mean zero and unit variance. The variable R_L, which also has a Gaussian distribution, is similarly defined from the inverse of the mean position of the energy deposition in three ECAL stacks. R_T and R_L are then related to the transverse and longitudinal behaviour of the shower in ECAL. For muon and hadron separation, two additional variables are introduced: $\overline{W}$, the average shower width in HCAL, and N_{10}, the penetration, i.e. the number of fired planes in the last ten HCAL planes. Both quantities are derived from the digital read–out of HCAL.

The usual procedure to identify particles is to cut on one or several of these variables. Here, a likelihood method to combine these variables and to produce the best estimate of the particle type has been developed along the following lines:

- Energy–dependent reference distributions of probability densities $f_i^j(x_i)$ are set up for variable x_i and particle type j.

- The probability is calculated for the considered particle to be of a given type. Using the reference distributions of the ith variable, a probability P^j is defined:

$$P^j = \frac{E^j}{\sum_j E^j}, \quad E^j = \prod_i \frac{f_i^j(x_i)}{\sum_j f_i^j(x_i)} . \tag{8}$$

- The particle is assigned to the particle type which has the largest probability. This assumes *a priori* an equal probability for the three particle types, which is not far from the real situation.

All the reference distributions have been established from Monte Carlo calculations. However, they have been checked, and sometimes slightly modified, with real data using events from $e^+e^- \to e^+e^-$, $\mu^+\mu^-$ with an electron or a muon tag, respectively, and $e^+e^- \to \tau^+\tau^-$, where one of the τ decays into $\rho\nu_\tau$ (the ρ in turn decays into a π^0 and a π, therefore giving a π for the hadron sample). These reactions provide an experimental check of the particle identification with clean samples of electrons, muons, and pions.

4.2 Identification of electrons from photon conversions

Electrons from converted photons are identified using dE/dx, R_L, and R_T so as to maximize statistics and to retain a high particle identification efficiency: below 2 GeV/c, a dE/dx measurement is required and is supplemented by R_L and R_T if they are available, and vice versa for the momentum range above 2 GeV/c. The corresponding track selection efficiency ε_{tr} (a measure of the availability of the requested information for the particle identification), the identification efficiency $\varepsilon_{e\to e}$, and the misidentification probability $\varepsilon_{q\to e}$ are given in Table 1.

Table 1: *Based on the simulated Monte Carlo $\tau^+\tau^-$ events, the track selection efficiency $\varepsilon_{\rm tr}$, the electron identification efficiency $\varepsilon_{e\to e}$, and the probability of another particle type to be identified as an electron, $\varepsilon_{q\to e}$ (in %), have been determined by the likelihood method.*

(GeV/c)	$\varepsilon_{\rm tr}$	$\varepsilon_{e\to e}$	$\varepsilon_{q\to e}$
p <2	87.65±0.47	99.55±0.16	0.49±0.13
$p \geq 2$	97.76±0.06	93.91±0.24	0.85±0.04

4.3 General particle identification

The general particle identification method is only applied to one–track τ candidates which satisfy the following three additional conditions:

1. The momentum of the track is larger than 2 GeV/c,

2. The track does not point to ECAL cracks or the overlap region between barrel and end–caps (resulting in an inefficiency of 15.8%),

3. The extrapolation of the track to HCAL does not point into a HCAL crack (8.5% inefficiency).

After these cuts, the overall track selection efficiency is 73.6%.

Fig.1 shows the distributions of three probabilities P_e, P_μ, and P_h for all one–prong τ candidates on a triangular plot. Good separation is achieved between the particle species, and the distributions for data are well reproduced by the Monte Carlo. The results of the general particle identification method applied to Monte Carlo are given in Table 2. Good agreement is found with experimental determinations, as discussed

Table 2: *The particle identification efficiencies $\varepsilon_{i\to i}$ ($i = e,\mu,h$) and misidentification probabilities $\varepsilon_{i\to j}$ ($i \neq j$, $j = e,\mu,h$) (in %), determined using the Monte Carlo $\tau^+\tau^-$ events. The particle types shown in the first row are those generated, in the first column those identified. Values are averaged for all momenta larger than 2 GeV/c.*

Id.↓ True →	e	μ	h
e	99.40±0.09	≤0.01	1.01±0.09
μ	≤0.01	99.12±0.10	1.50±0.11
h	0.60±0.09	0.88±0.10	97.49±0.14

below.

4.4 Checks on the particle identification procedure with known samples

The selected samples of electrons, muons, and pions discussed in section 4.1 can be used to check the contamination probabilities. Fig.2 gives the corresponding distributions of the probabilities P_e, P_μ, and P_h showing the expected peaks for the selected particles. The small contributions seen for the other particle types are the result of misidentification and of the small $\tau^+\tau^-$ contamination in the e^+e^- and $\mu^+\mu^-$ samples.

Table 3 gives a more quantitative comparison of the contaminations.

The agreement is satisfactory, except for the separation between muons and hadrons where the small differences are caused mostly by the imperfect simulation of HCAL for penetrating particles. The effect is relatively minor and is included in the systematic error.

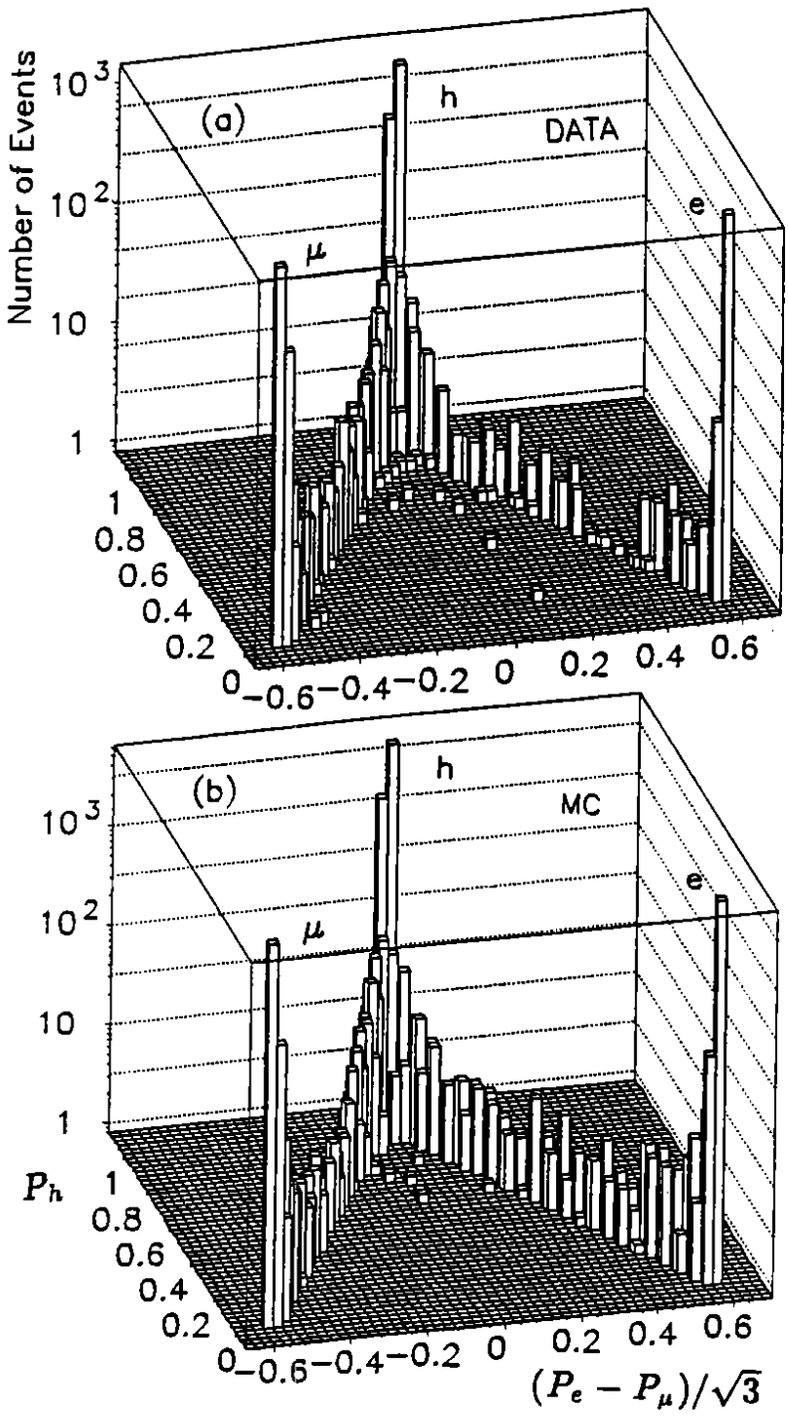

Figure 1: *The triangular plot for the probabilities P_e, P_μ, and P_h in $\tau^+\tau^-$ events for (a) data and (b) Monte Carlo.*

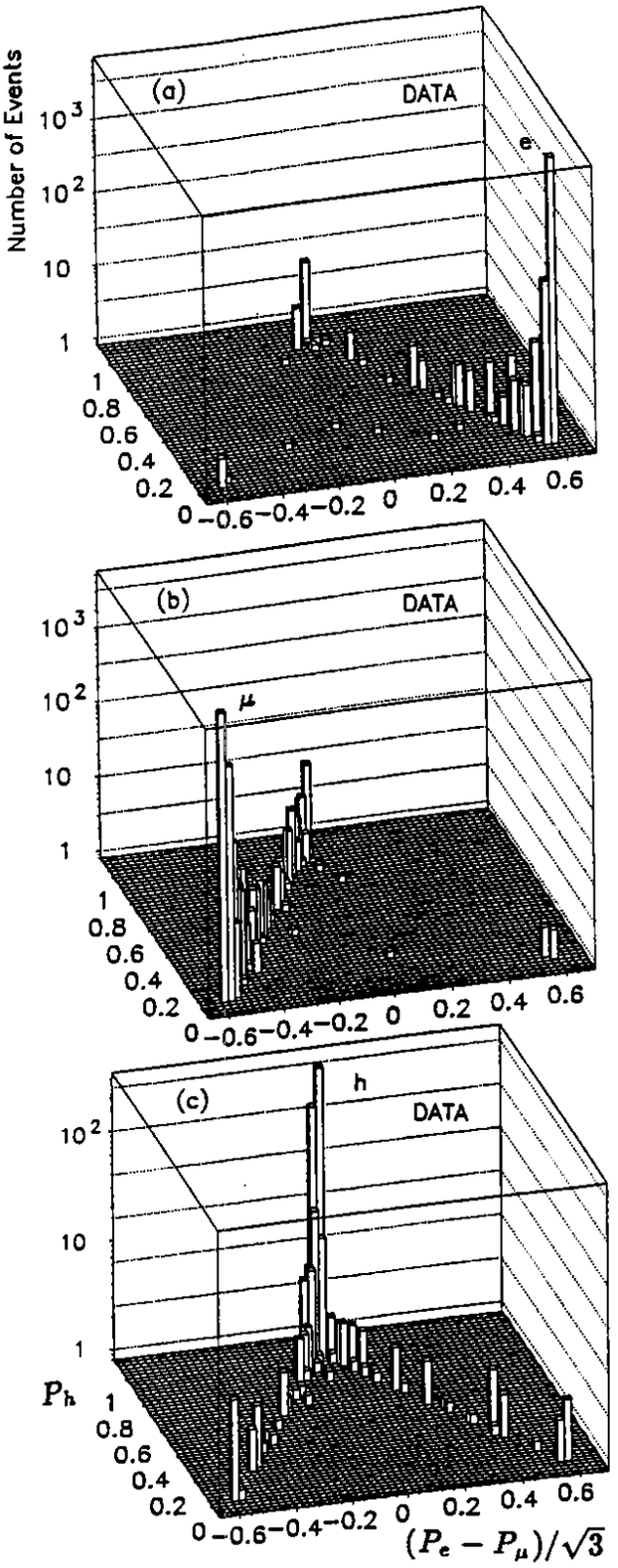

Figure 2: *The triangular plot for the probabilities P_e, P_μ, and P_h in the different data samples: (a) e^+e^-, (b) $\mu^+\mu^-$, and (c) $\pi(\tau \to \rho)$.*

Table 3: *Data and Monte Carlo comparison of the particle identification efficiencies $\varepsilon_{i\to i}$ (i = e,μ,h) and misidentification probabilities $\varepsilon_{i\to j}$ ($i \neq j$) (in %) determined on the selected samples of electrons, muons, and rhos.*

data				
Id.↓	True →	e	μ	h
e		99.32 ± 0.10	0.07 ± 0.03*	1.55 ± 0.44
μ		0.04 ± 0.02*	98.72 ± 0.13	2.32 ± 0.54
h		0.64 ± 0.09	1.21 ± 0.13	96.13 ± 0.69
Monte Carlo				
Id.↓	True →	e	μ	h
e		99.43 ± 0.15	≤ 0.03	1.47 ± 0.19
μ		≤ 0.04	99.38 ± 0.14	1.64 ± 0.20
h		0.57 ± 0.15	0.62 ± 0.14	96.89 ± 0.27

* *Consistent with $\tau^+\tau^-$ background in e^+e^- and $\mu^+\mu^-$ samples.*

5 Photon and Neutral Pion Reconstruction

Since about 40% of τ decays have at least one π^0 in the final state, it is essential to reconstruct efficiently photons and π^0's for the measurement of the quasi–exclusive and exclusive τ branching ratios. Due to the large Lorentz boost, the photons from one or several neutral pions generate showers in ECAL which are in most cases very close to each other or to showers from charged hadrons. To provide a check on the estimate of systematic uncertainties, two different methods have been developed to identify photons in such a dense environment.

Both identification procedures begin with a search for local maxima among the towers of the first two stacks of ECAL in a cone of 30° half–angle around the thrust axis computed with the charged tracks only. A maximum tower contains more energy than any of its immediate neighbours. Two definitions are used: in a strict definition neighbouring towers must have a common face(method A), whereas in a looser definition neighbouring towers share a face or a single corner(method B). Each local maximum represents the first tower of a separate cluster. It must have a distance of more than 4 cm from the impact point of a charged particle if the cluster is to be considered as a photon candidate.

The full reconstruction of the clusters and the assignment of energies start from the local maxima. In method A, the remaining towers are assigned in order of decreasing energy, adding the energy of a tower to the same cluster as its highest energy neighbour. Method B shares the energy of a tower between adjacent clusters using an algorithm based on the expected radial distributions for electromagnetic showers normalized to the energies of the local maxima. In both methods, photon candidates are required

to have clusters extending in depth over at least two stacks in order to reject satellite clusters of hadronic showers. The minimum cluster energy is 250 MeV. This threshold is raised to 1 GeV if the photon shower overlaps with a cluster that is linked to the track of a charged particle, and an additional threshold of 100 MeV is required in the first stack.

The two algorithms for photon finding yield compatible results on branching ratios. The differences are consistent with our estimate of possible systematic effects. The results quoted here are those obtained with method A.

Fig.3(a) shows the photon multiplicity distribution for a τ decay, in good agreement with the τ Monte Carlo expectation using the final branching ratios determined in this analysis. The high multiplicity tail is expected from the small $Z^0 \to q\bar{q}$ contamination. The energy spectra are also in good agreement down to 0.25 GeV (Fig.3(b)). The possible discrepancy around 1 GeV could be due to shortcomings in the Monte Carlo simulation of hadron interactions in ECAL leading to fake photon candidates. Variations of the two main thresholds from 0.25 to 0.5 GeV, and from 0.5 to 2 GeV, respectively, give only small differences in the branching ratios, which have been included in the systematic uncertainties.

A fraction of the converted photons is recovered and added to those found in ECAL. First, pairs of identified electrons and positrons are combined if their invariant masses are smaller than 100 MeV/c^2. Then, unassociated electrons or positrons in multi-prong decays are assumed to originate from asymmetric conversions and are assigned to photons of the same energies.

Detailed checks on the Monte Carlo simulation of photon conversions have been performed. The fraction of reconstructed photons coming from conversions in one-prong τ decays with at least one photon is found to be 0.0784 ± 0.0037 in the data. The corresponding Monte Carlo value is 0.0711 ± 0.0017. As an example, Fig.4 shows the distribution of the distance between the conversion point and the interaction region. The general agreement between data and Monte Carlo indicates that both the description of the material around the beam pipe and in the inner wall of the TPC, and the understanding of the track geometrical cuts are adequate. The small excess of converted photons in the data with respect to the simulation has been accounted for in the estimate of systematic errors.

The distribution of the invariant mass $m_{\gamma\gamma}$ for all final states with at least two reconstructed photons is shown in Fig.5. A clear π^0 signal is seen with good agreement between Monte Carlo and data. The mass range for accepted π^0 candidates is $0.07 < m_{\gamma\gamma} < 0.21$ GeV/c^2. When a photon is shared by distinct π^0 candidates, the combination with a mass closer to m_{π^0} is chosen.

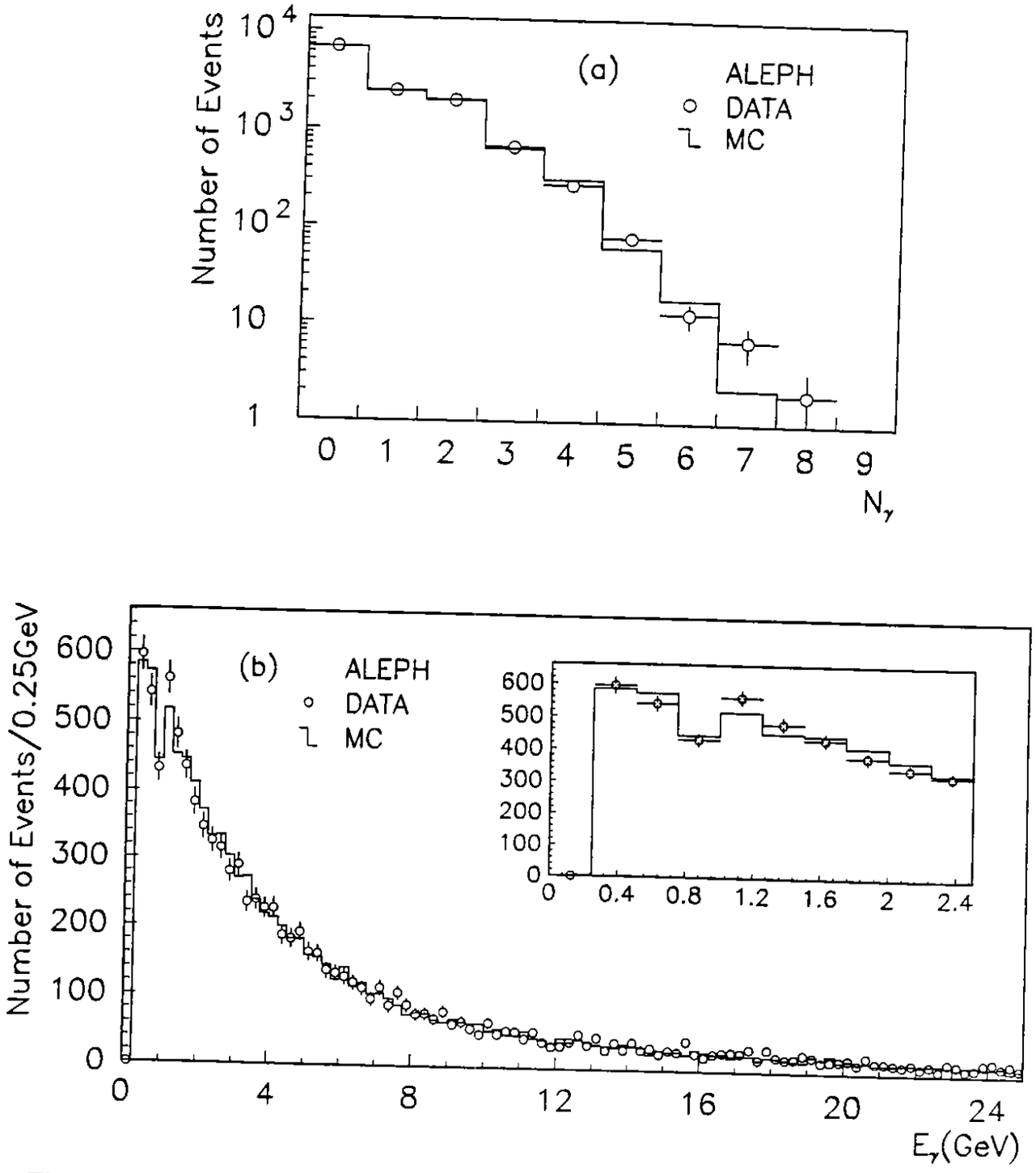

Figure 3: *(a): the photon multiplicity distribution of τ decays; (b): the energy spectrum of the reconstructed photons. The histograms correspond to the τ Monte Carlo.*

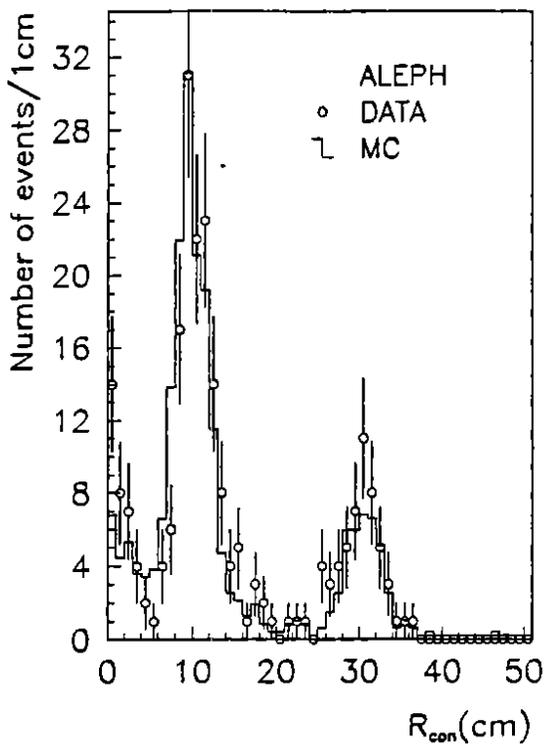

Figure 4: *The distance of the reconstructed conversion point to the beam axis of* e^+e^- *pairs.*

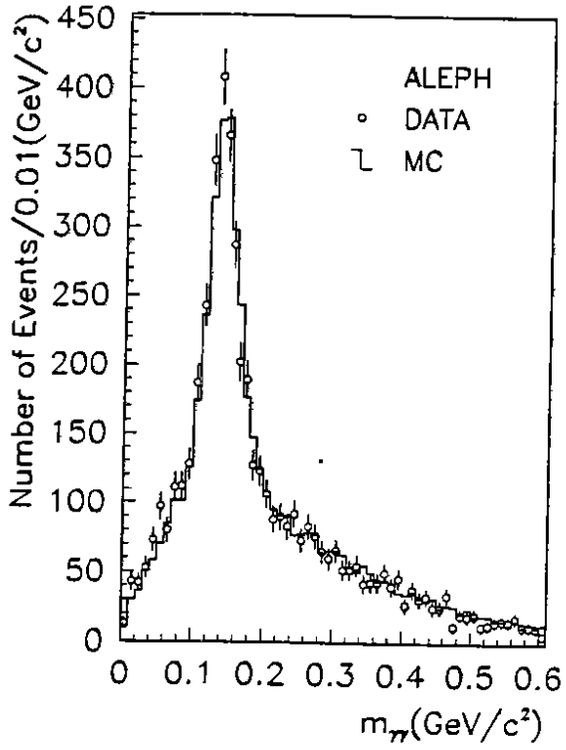

Figure 5: *The invariant mass $m_{\gamma\gamma}$ in all combinations for events with at least two reconstructed photons.*

6 Monte Carlo Generator for Tau Production and Decays

The Monte Carlo generator KORALZ[13] is used to generate $\tau^+\tau^-$ events in the Z^0 energy range. The production includes initial state radiation up to order α^2 with multiple photon emission obtained through exponentiation, and final state radiation and electroweak corrections both to order α. No interference between initial and final state radiation is allowed in the case where multiple photon emission occurs in the initial state.

Monte Carlo generated $\tau^+\tau^-$ events decay according to the decay library TAUOLA[14] which includes the following modes: $\tau \to e\bar{\nu}_e\nu_\tau$, $\mu\bar{\nu}_\mu\nu_\tau$, $\pi\nu_\tau$, $K\nu_\tau$, $\rho\nu_\tau$, $K^*\nu_\tau$, $a_1\nu_\tau$, $4\pi\nu_\tau$, $5\pi\nu_\tau$, and $6\pi\nu_\tau$. The matrix elements for the first six channels are well known theoretically. The a_1 is known phenomenologically and decays into $\rho\pi$[15], giving three charged π's or one charged π and two π^0's in equal amounts. The last three multipion decays are generated according to a simplified matrix element following phase space which, contrary to the other modes, does not include spin effects and therefore correlations between the two τ decays. Finally, for the first seven modes, single photon radiation is included in the decay processes in the leading logarithmic approximation[16].

The branching ratios used in KORALZ are close to the world averages. However, our method does not rely on their particular values.

7 Absolute Normalization of Tau Pair Event Sample

Assuming lepton universality in the Z^0 decays, the number of produced $\tau^+\tau^-$ events can be derived from the corresponding number of electron and muon pairs. The cross sections for lepton–pair production have been measured on the same data sample[12]. For convenience, the ratio of hadrons to electrons and muons is used to obtain an absolute normalization for the $\tau^+\tau^-$ pair production.

The hadronic events from the same runs as used in the $\tau^+\tau^-$ analysis are selected as described in Ref.[12], taking into account the selection efficiency, the estimated background and their systematic uncertainties. The average of the measured values of the Z^0 partial widths into electrons and muons:

$$\frac{\Gamma_{\rm had}}{\Gamma_{l^+l^-}} = 21.00 \pm 0.22 \ , \tag{9}$$

is taken from Ref.[12]. Including a correction of 1.2% to take into account the photon exchange contribution under the Z^0 peak, the number of $\tau^+\tau^-$ events which is used for the normalization of our sample is given by:

$$N_{\tau^+\tau^-} = 8538 \pm 89 \ . \tag{10}$$

8 The Topological Branching Ratios

8.1 The method

The charged–track topology of a $\tau^+\tau^-$ pair event should be $ij\,(i,j=1,3,5)$. However, in practice, the topology of a detected $\tau^+\tau^-$ pair event is $kl(k,l=1,2,...)$. This is due to the fact that (a) tracks may be lost because they overlap, escape detection, or interact; and (b) additional tracks may appear from converted photons and hadron interactions. In order to reduce the contamination, additional cuts are made on tracks from the event selection:

- The cut on the transverse distance to the beam axis is tightened to 0.5 cm.
- It is required that the relevant information is available for electron identification for all tracks. Electrons are identified by the method described in section 4.2.
- Identified electrons are removed if they are not the only track left in each decay.

Neither photon reconstruction nor the general particle identification method are used for this analysis.

The true number N_{ij} of $\tau^+\tau^-$ pairs where one τ decays into i and the other into j charged particles is related to the number of $\tau^+\tau^-$ pair candidates n_{kl} expected to be seen in the detector by:

$$\begin{aligned} n_{kl} &= n_{kl}^{\mathrm{bkg}} + \sum_{i\le j} T_{ij\to kl} N_{ij} \quad (k,l=1,2,3,...)\,, \\ N_{ij} &= (2-\delta_{ij}) N_{\tau^+\tau^-} B_i^T B_j^T \quad (i,j=1,3,5)\,. \end{aligned} \tag{11}$$

$N_{\tau^+\tau^-}$ is the total number of produced $\tau^+\tau^-$ pairs, and B_i^T is the topological branching ratio for the decay into i charged particles. $T_{ij\to kl}$ represents the probability for reconstructing $\tau^+\tau^-$ pairs with charge topology ij as $\tau^+\tau^-$ pairs with topology kl. Finally, n_{kl}^{bkg} is the number of expected non–$\tau^+\tau^-$ background events in the kl topology, obtained from the different Monte Carlo generators.

The Monte Carlo determined mixing matrix T is given in Table 4. It includes the selection acceptance and the track selection efficiencies required for electron identification. It is largely diagonal for small multiplicities. The $\tau^+\tau^-$ topologies with high track multiplicities are somewhat distorted by the overall multiplicity cut ≤ 6 tracks used in the selection. The relatively lower efficiencies for three–prong decays are due to the missing mass cut (8) in the selection procedure. Even-even topologies are expected at a very small rate.

The final data sample consists of 5095 $\tau^+\tau^-$ candidates. Assuming the number m_{kl} of events actually observed in the detector is Poisson–distributed around the expectation n_{kl}, then the parameters B_1^T, B_3^T, and B_5^T can be obtained by a likelihood method.

Table 4: *The mixing matrix T determined by Monte Carlo. The matrix elements are given in % and the quoted errors are statistical.*

$kl \setminus ij$	11	13	15	33
11	66.99 ± 0.30	2.07 ± 0.16	≤ 1.79	0.28 ± 0.20
12	0.54 ± 0.05	7.83 ± 0.30	5.36 ± 3.01	0.28 ± 0.20
13	0.19 ± 0.03	48.76 ± 0.55	12.50 ± 4.42	2.81 ± 0.62
14	0.01 ± 0.01	0.02 ± 0.02	17.86 ± 5.12	≤ 0.14
15	≤ 0.01	≤ 0.01	21.43 ± 5.48	≤ 0.14
22	≤ 0.01	0.01 ± 0.01	≤ 1.79	0.98 ± 0.37
23	≤ 0.01	0.07 ± 0.02	≤ 1.79	9.54 ± 1.10
24	≤ 0.01	≤ 0.01	≤ 1.79	≤ 0.14
33	≤ 0.01	0.04 ± 0.02	≤ 1.79	25.39 ± 1.63

8.2 Study of systematic effects

Several effects can alter the charged–particle multiplicity. The uncertainty in the event selection has been found to be one of the dominant systematic sources of error. The effect due to the subtraction of non–$\tau^+\tau^-$ background has been studied in the different topologies by varying the number of the non–$\tau^+\tau^-$ background events estimated from the various Monte Carlo generators. The electron identification procedure introduces possible biases at the level of the track selection efficiency and of the misidentification probabilities. These effects have been estimated by comparing Monte Carlo and data samples of pure particle types, as described in section 4.

The quality of the simulation of hadron interactions in the material near the beam pipe has been checked to be sufficient for our purpose: no significant effect was seen in the results when the transverse distance cut of tracks was varied between 0.5 and 2 cm. Increasing this cut has the effect of accepting more tracks which are scattered before being detected in the TPC.

Multi–prong τ decays lead to close overlapping tracks in the TPC. Special attention was given to the case where two overlapping tracks were lost because of reconstruction problems. This effect gives the dominant contribution to the mixing matrix element $T_{13\to 11}$. Its systematic uncertainty is estimated to be 0.48% by detailed comparison of relevant distributions of the events in data and Monte Carlo and by event scanning. This results in a systematic uncertainty of 0.10% and 0.12% for B_1^T and B_3^T, respectively.

Because of the $\tau^+\tau^-$ selection cuts, the efficiency for the hadronic τ decays varies slowly with the hadronic mass. Any discrepancy between data and Monte Carlo in the mass distribution could result in a slightly incorrect efficiency calculation. As such an effect is observed for the a_1 channel (section 9.2), a corresponding systematic uncertainty has been included.

Systematic effects from decays involving $K_S^0 \to \pi^+\pi^-$ are negligible since the corre-

sponding branching ratio is small ($\sim 0.5\%$) and their efficiency is not expected to be very different from that of non–K^0_S decays.

Table 5 summarizes the systematic uncertainties for the measurement of the topological branching ratios.

Table 5: *Systematic uncertainties of topological branching ratios(in %).*

Sources	ΔB_1^T	ΔB_3^T	ΔB_5^T
event selection	0.40	0.06	—
non–$\tau^+\tau^-$ background	0.12	0.04	0.02
selection for electron identification	0.16	0.09	0.01
tracking	0.10	0.12	—
γ conversions	0.06	0.06	0.01
Monte Carlo generator	0.15	0.15	—
Combined error	0.48	0.23	0.03

8.3 Results

The likelihood fit of the observed distribution of multiplicities yields the following results for the topological branching ratios in %:

$$\begin{aligned} B_1^T &= 85.45^{+0.69}_{-0.73} \pm 0.48 \ , \\ B_3^T &= 14.35^{+0.40}_{-0.45} \pm 0.23 \ , \\ B_5^T &= 0.10^{+0.05}_{-0.04} \pm 0.03 \ , \end{aligned} \tag{12}$$

where the first uncertainty is statistical and the second systematic. A common relative uncertainty of $\pm 0.52\%$ should be added to take into account the normalization of the $\tau^+\tau^-$ sample. The purely statistical correlation factor between B_1^T and B_3^T is found to be $\rho = -0.27$ (the systematic contribution is small).

As a check on the quality of the fit, the observed and fitted multiplicity distributions are given in Table 6. The good agreement observed confirms the correct simulation of the data(conversions, interactions, track reconstruction) in the Monte Carlo calculations and the proper evaluation of non–$\tau^+\tau^-$ backgrounds. The momentum distribution of the one–prong candidates agrees well with the Monte Carlo simulation (Fig.6.).

8.4 Limit on undetected τ decays

From the absolute determination of τ branching ratios from the $\tau^+\tau^-$ sample, it is possible to investigate the existence of new decay modes which would be undetected by our analysis. Such a possibility would require special properties of these decay modes

Table 6: *A comparison of the charged track multiplicity between data and the Monte Carlo using the fitted branching ratios. The quoted errors are statistical only.*

kl	$\tau^+\tau^-$ MC	non$-\tau^+\tau^-$ bkg	MC total	Data
11	3812.6 ± 14.3	135.1 ± 26.9	3947.7 ± 30.5	3939
12	172.3 ± 6.3	1.8 ± 1.0	174.1 ± 6.4	202
13	908.5 ± 13.1	0.7 ± 1.0	909.2 ± 13.1	889
14	3.2 ± 0.8	0.1 ± 1.0	3.3 ± 1.3	4
15	3.0 ± 0.8	≤ 1.0	3.0 ± 1.3	2
22	2.1 ± 0.7	≤ 1.0	2.1 ± 1.2	2
23	19.7 ± 2.2	5.1 ± 1.9	24.8 ± 2.9	18
24	≤ 0.2	≤ 1.0	≤ 1.0	0
33	39.7 ± 3.1	1.0 ± 1.0	40.7 ± 3.3	39

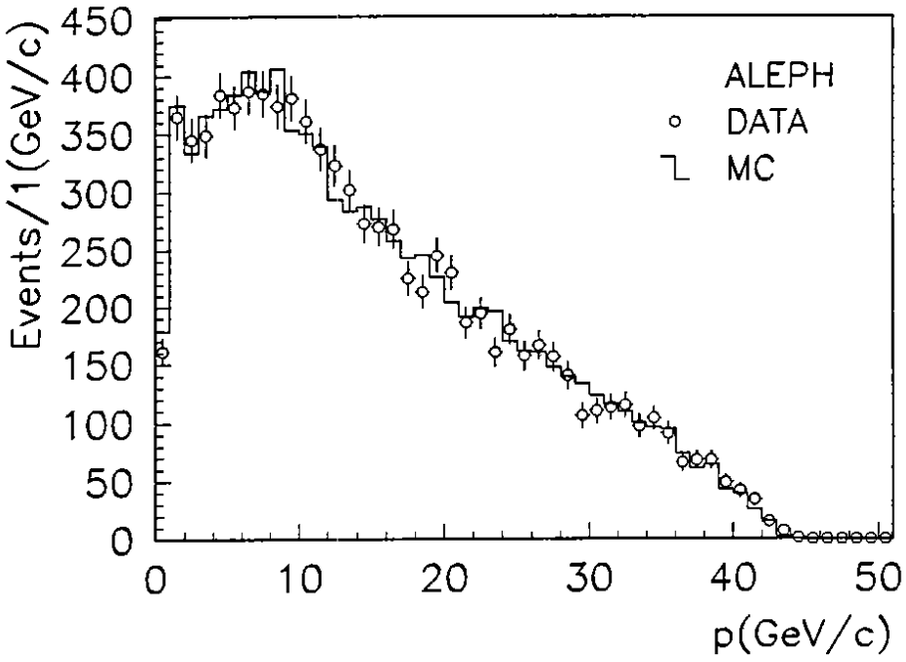

Figure 6: *The momentum distributions of the charged particles for the one–prong decays both for data and for Monte Carlo.*

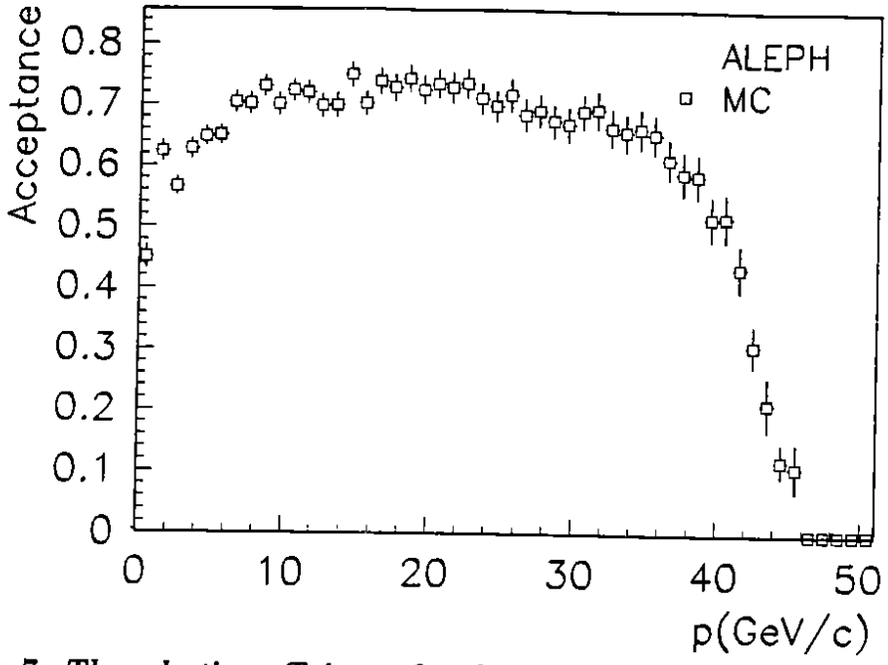

Figure 7: *The selection efficiency for the one–prong decays as a function of the momentum of the charged particles.*

owing to our broad–band momentum acceptance(Fig.7). One could imagine the case, for example, where the τ decayed into eN, N being a neutrino–like particle almost mass–degenerate with the τ itself, so that the small momentum electron would escape detection.

To bound the branching fraction of such peculiar modes, it is useful to consider if the measured branching ratios represent a complete set. The measured sum

$$\sum_{i=1,3,5} B_i^T = 99.9 \pm (0.70)_{\rm stat} \pm (0.51)_{\rm syst} \pm (0.52)_{\rm norm}\ (\%) \qquad (13)$$

is consistent with 100%. Since this result assumes lepton universality in the Z^0 decays, there is still the possibility that a new undetected τ decay mode is exactly compensated by a deviation from universality of the τ coupling to the Z^0.

Under the assumption of lepton universality in the neutral current, a 95% CL limit can be set for totally undetected modes

$$B_{\rm undetected} < 2.1\% \ . \qquad (14)$$

9 Quasi–exclusive Branching Ratios

9.1 The method

In this analysis, each reconstructed τ decay is classified according to the number of charged particles, their type, the number of photons and π^0's reconstructed from photon pairs. Eight classes are thus defined (Table 7).

Table 7: *Definition of quasi–exclusive channels. The presence of radiative photons in the decays does not change the input Monte Carlo classification.*

class	final states X for $\tau \rightarrow X\nu_\tau$	reconstruction criteria		input MC classification
		particle type	number of photons	
1	$e\overline{\nu}_e$	$\geq 1e$	any	$e\overline{\nu}_e$
2	$\mu\overline{\nu}_\mu$	$1\ \mu$	any	$\mu\overline{\nu}_\mu$
3	h	1 hadron	0	π, K, $K^* \rightarrow K^0_L\pi$, $K^* \rightarrow \pi K^0_S(\rightarrow \pi^+\pi^-)$
4	$h\pi^0$	1 hadron	1, 2 with $1\pi^0$	$\pi\pi^0$,$K^* \rightarrow K\pi^0$
5	$h2\pi^0$	1 hadron	2, 3 with $1\pi^0$, 4 with $2\pi^0$	$\pi 2\pi^0$, $K^* \rightarrow \pi K^0_S(\rightarrow \pi^0\pi^0)$
6	$h \geq 3\pi^0$	1 hadron	3, 4 with $1\pi^0$,≥ 5	$\pi \geq 3\pi^0$
7	$3h$	≥ 2 hadrons	0	3π
8	$3h \geq 1\pi^0$, $5h \geq 0\pi^0$	≥ 2 hadrons	≥ 1	$3\pi \geq 1\pi^0$, $5\pi \geq 0\pi^0$

Not only is this definition general but also complete in the sense that all τ decays selected by the analysis are classified.

It is clear from section 6 that the Monte Carlo generation includes more physics possibilities than our scheme permits: Cabibbo-suppressed decays involve charged kaons that we do not attempt to separate from pions, as well as neutral kaons. Although some possibility exists to identify K^0_L's in HCAL, this is not implemented in this analysis. The situation is different for K^0_S's: decays into $2\pi^0$ are readily identified, while for $\pi^+\pi^-$ decays, the information on possible secondary vertices is not used at present (this can be improved when the need comes with more statistics). These problems are taken into account in our procedure which relies on the Monte Carlo to simulate the corresponding reconstruction efficiencies. Since τ decays involving $K^0_S \rightarrow \pi^+\pi^-$ are only at the 0.5% level, the risk of producing large systematic effects is excluded.

The set of simulated τ decay channels, as shown in Table 7, may not be complete. For instance the decay mode $\eta\pi\pi^0$ is not included. However, such channels would lead to final states already included in our classification and consequently would be taken into account although possibly with an incorrect efficiency. Furthermore, the corresponding branching fractions should be of order 10^{-3} according to our present

knowledge[4,6], and therefore all related effects are expected to be small compared to the statistical uncertainty.

The strategy to classify a reconstructed τ candidate is the following:

1. If there is only one charged track: the general particle identification method is used and the decay is classified in one of the first six classes depending on the identified particle type and the number of π^0's or γ's.

2. If there is more than one charged track: electrons are first identified and then transformed into photon candidates according to the prescription given in section 4. If all charged particles happen to be identified as electrons, the event is in class 1, and the highest energy particle is assumed to be the primary electron in the τ decay. Otherwise, the candidate is classified according to the number of hadrons and the number of reconstructed photons.

Due to the particle identification inefficiency and misidentification probabilities, and due to the photon reconstruction inefficiency, some mixing occurs and the true number $N_i(= N_\tau B_i)$ of decay events in class i is related to the expected number n_j of decay events in reconstructed class j by:

$$n_j = n_j^{\rm bkg} + N_\tau \sum_i E_{i\to j} B_i \quad (i,j = 1,...,8) \ , \tag{15}$$

in which N_τ is the total number of produced τ decays, B_i are the branching ratios to be measured, the mixing matrix elements $E_{i\to j}$ give the probability of generated class i being reconstructed as class j, and $n_j^{\rm bkg}$ is the number of non$-\tau$ background events obtained by Monte Carlo. Part of the background estimated at the selection level is significantly reduced by the particle identification criteria. Note that the τ Monte Carlo enters only via the mixing matrix E whose elements are independent of the input branching ratios except for the rare K and K^* channels.

The matrix E is given in Table 8. It is mostly diagonal as a result of good particle identification and π^0 reconstruction capabilities. Some mixing is observed between classes with π^0's, reflecting the difficulty of detecting a large photon multiplicity clustered around a charged track. It is important to notice that the overall efficiency in each class is large and rather uniform because of the looseness of the cuts used in the analysis.

The final data sample selected to ensure full particle identification for the quasi–exclusive analysis consists of 8429 τ candidates. Note that this sample of τ decays does not require that the full $\tau^+\tau^-$ event be reconstructed and identified. Consequently the samples used for the topological and quasi–exclusive analyses partly overlap: 2899 complete $\tau^+\tau^-$ events are used in both analyses, with an additional sample of 1914 events where only one of the two τ's is kept for the quasi–exclusive analysis. The remaining parts of the two samples do not overlap. Assuming $n_j^{\rm obs}$ is the number of observed τ candidates in class j, then the branching ratios B_i can be straightforwardly derived from Eq.(15).

Table 8: *The mixing matrix $E_{i\to j}$, giving the probabilities for assigning a τ decay in class i to class j. The matrix elements are given in %. The generated class types are in the first row, and the identified class types in first column.*

$j\downarrow\ i\to$	1	2	3	4
1	49.89 ± 0.45	0.01 ± 0.01	0.59 ± 0.08	0.66 ± 0.06
2	≤ 0.01	56.30 ± 0.45	0.60 ± 0.08	0.69 ± 0.07
3	0.24 ± 0.04	0.44 ± 0.06	45.95 ± 0.54	2.13 ± 0.12
4	0.15 ± 0.04	0.10 ± 0.03	3.78 ± 0.21	41.74 ± 0.39
5	0.03 ± 0.02	0.02 ± 0.01	0.46 ± 0.07	5.55 ± 0.18
6	≤ 0.01	≤ 0.01	0.10 ± 0.05	0.33 ± 0.05
7	0.01 ± 0.01	0.02 ± 0.01	1.06 ± 0.11	0.04 ± 0.02
8	≤ 0.01	0.01 ± 0.01	0.32 ± 0.06	0.55 ± 0.06
sum	50.32 ± 0.45	56.91 ± 0.45	53.18 ± 0.54	52.24 ± 0.40

continued	5	6	7	8
1	0.88 ± 0.13	1.06 ± 0.18	≤ 0.02	≤ 0.02
2	0.49 ± 0.09	0.36 ± 0.10	≤ 0.02	≤ 0.02
3	0.71 ± 0.11	≤ 0.03	0.57 ± 0.10	≤ 0.02
4	6.85 ± 0.35	1.75 ± 0.23	0.34 ± 0.08	0.34 ± 0.09
5	33.45 ± 0.64	14.59 ± 0.61	0.13 ± 0.05	0.22 ± 0.07
6	7.00 ± 0.35	27.34 ± 0.77	≤ 0.02	≤ 0.02
7	≤ 0.02	≤ 0.03	48.99 ± 0.69	5.36 ± 0.34
8	0.93 ± 0.13	1.06 ± 0.18	7.41 ± 0.36	54.01 ± 0.75
sum	50.31 ± 0.68	46.17 ± 0.87	57.76 ± 0.68	60.48 ± 0.73

9.2 Study of systematic effects

Many sources of systematic uncertainties have been considered for the measurement of the branching ratios of the individual channels. Some of them have been discussed in the previous sections.

An important source arises from the photon reconstruction. The corresponding uncertainty has been estimated by varying all relevant parameters (cluster thresholds, proximity to the charged track, π^0 mass cut) within reasonable ranges. Possible statistical effects are also introduced in this procedure. Since they have not been subtracted out, the estimate is considered to be conservative.

The possible misclassification of the small residual hadronic background estimated from the Monte Carlo simulation has been taken into account in the non–τ background uncertainties.

An additional source of uncertainty could come from τ physics itself since the computation of the efficiency matrix relies on the proper Monte Carlo generation[13] of the kinematic distributions. Whereas the main channels (e, μ, π, ρ, a_1, K, K^*) are reasonably free of theoretical uncertainties, some biases could be expected in the less known channels ($\pi 3\pi^0$, $3\pi\pi^0$, 5π, ...). In fact, such a difference is noticed in the $3\pi\pi^0$ channels (class 8) where ω production is observed in the data but is not included in the generator. The corresponding systematic uncertainty has been estimated from the channel efficiencies obtained assuming different final states.

The various systematic uncertainties are summarized in Table 9.

In order to compare the reconstructed classes in data and Monte Carlo, $E_{\rm charged}/E_{\rm beam}$ distributions are plotted for classes 1 – 3 (Fig.8) and invariant mass distributions of all detected particles are shown for the other classes (Fig.9). Good agreement is found, except for the 3π(in class 7) and $\pi 2\pi^0$(in class 5) mass distributions where the observed mass shift is due to an inaccurate description of the a_1 resonance in the Monte Carlo. Our 3π mass distribution agrees with previous measurements, in particular with the precise determination of Ref.[15]. This effect has been included in the estimate of systematic uncertainties for the Monte Carlo physics simulation.

9.3 Results

The results for the quasi–exclusive branching ratios are given in Table 10. It must be emphasized that, because of the significant mixing between classes with π^0's, some correlation is expected between the corresponding branching ratios. The strongest statistical correlation ($\rho = -0.65$) is observed between B_5 and B_6.

The sum of the measured branching ratios is again consistent with completeness:

$$\sum_{i=1}^{8} B_i = 100.4 \pm (1.3)_{\rm stat} \pm (0.9)_{\rm syst} \pm (1.0)_{\rm norm}\ \% \ , \qquad (16)$$

and, in particular, we find that the sum of one–prong channels (taking into account the

Table 9: *Systematic uncertainties of quasi–exclusive branching ratios.*

1. *γ/π^0 reconstruction,*
2. *non–τ background subtraction,*
3. *particle identification,*
4. *detector simulation (selection, momentum cut, conversions, tracking),*
5. *Monte Carlo physics simulation.*

$\Delta B_i(\%)$	Sources					Total
class	1	2	3	4	5	
1	0.12	0.19	0.30	0.16	—	0.41
2	0.04	0.12	0.29	0.09	—	0.33
3	0.23	0.08	0.16	0.07	—	0.30
4	0.61	0.10	0.52	0.22	—	0.84
5	0.74	0.18	0.22	0.10	0.15	0.81
6	0.41	0.19	0.03	0.03	0.08	0.46
7	0.50	0.10	0.31	0.07	0.15	0.62
8	0.50	0.15	0.36	0.04	0.15	0.65

Table 10: *Results for the quasi–exclusive branching ratios. A common relative uncertainty of 1.0% should be added to take into account the normalization of the τ sample.*

class i		$B_i(\%)$
1	$e\overline{\nu}_e$	18.09±0.45±0.41
2	$\mu\overline{\nu}_\mu$	17.35±0.41±0.33
3	h	13.32±0.44±0.30
4	$h + (\pi^0, \gamma)$	25.02±0.64±0.84
5	$h + (2\pi^0, \pi^0\gamma, 2\gamma)$	10.53±0.66±0.81
6	$h + (3\pi^0 \geq 0\gamma, 2\pi^0 \geq 1\gamma, \pi^0 \geq 2\gamma, \geq 3\gamma)$	1.53±0.40±0.46
7	$3h$	9.49±0.36±0.62
8	$3h+ \geq 1(\pi^0, \gamma)$, $5h+ \geq 0(\pi^0, \gamma)$	5.05±0.29±0.65

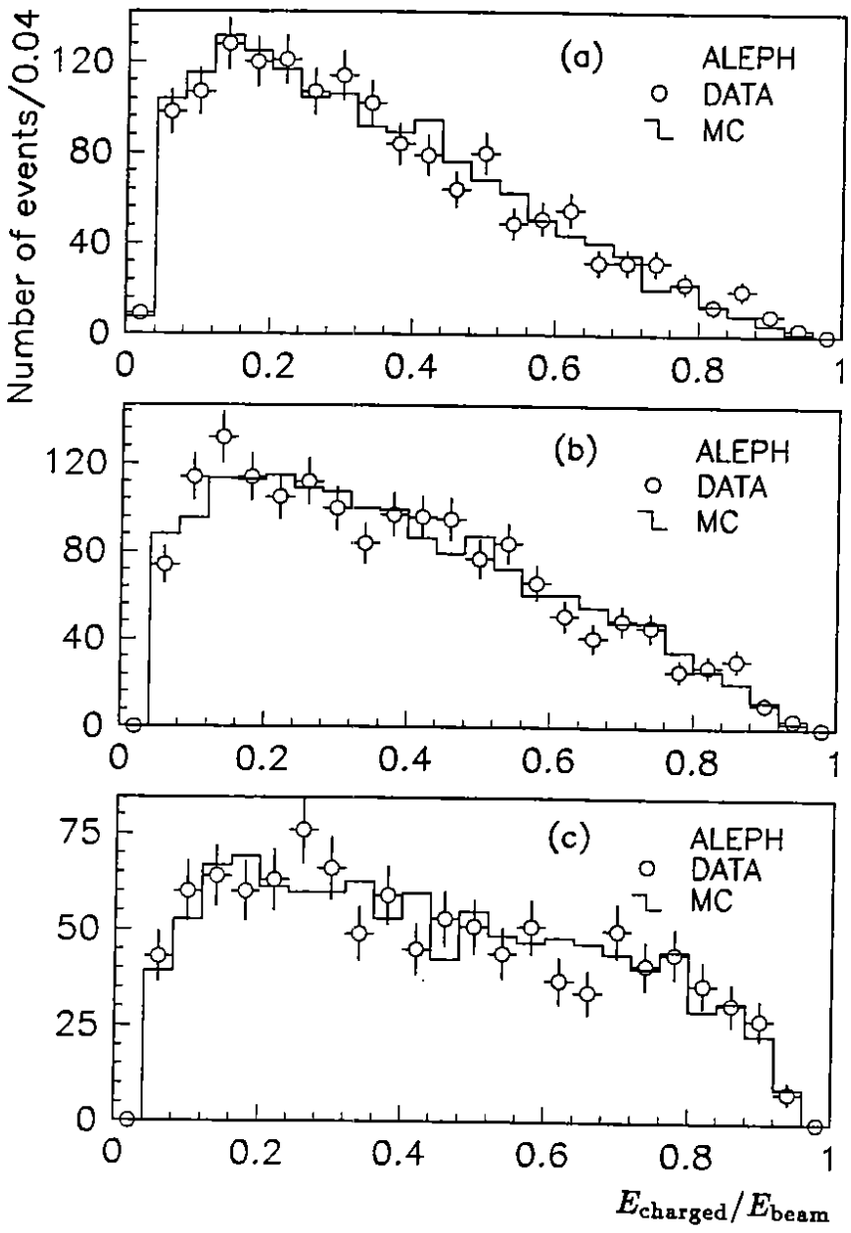

Figure 8: $E_{\mathrm{charged}}/E_{\mathrm{beam}}$ *distributions (a) – (c) for classes 1 – 3, respectively, in the quasi–exclusive branching ratio analysis.*

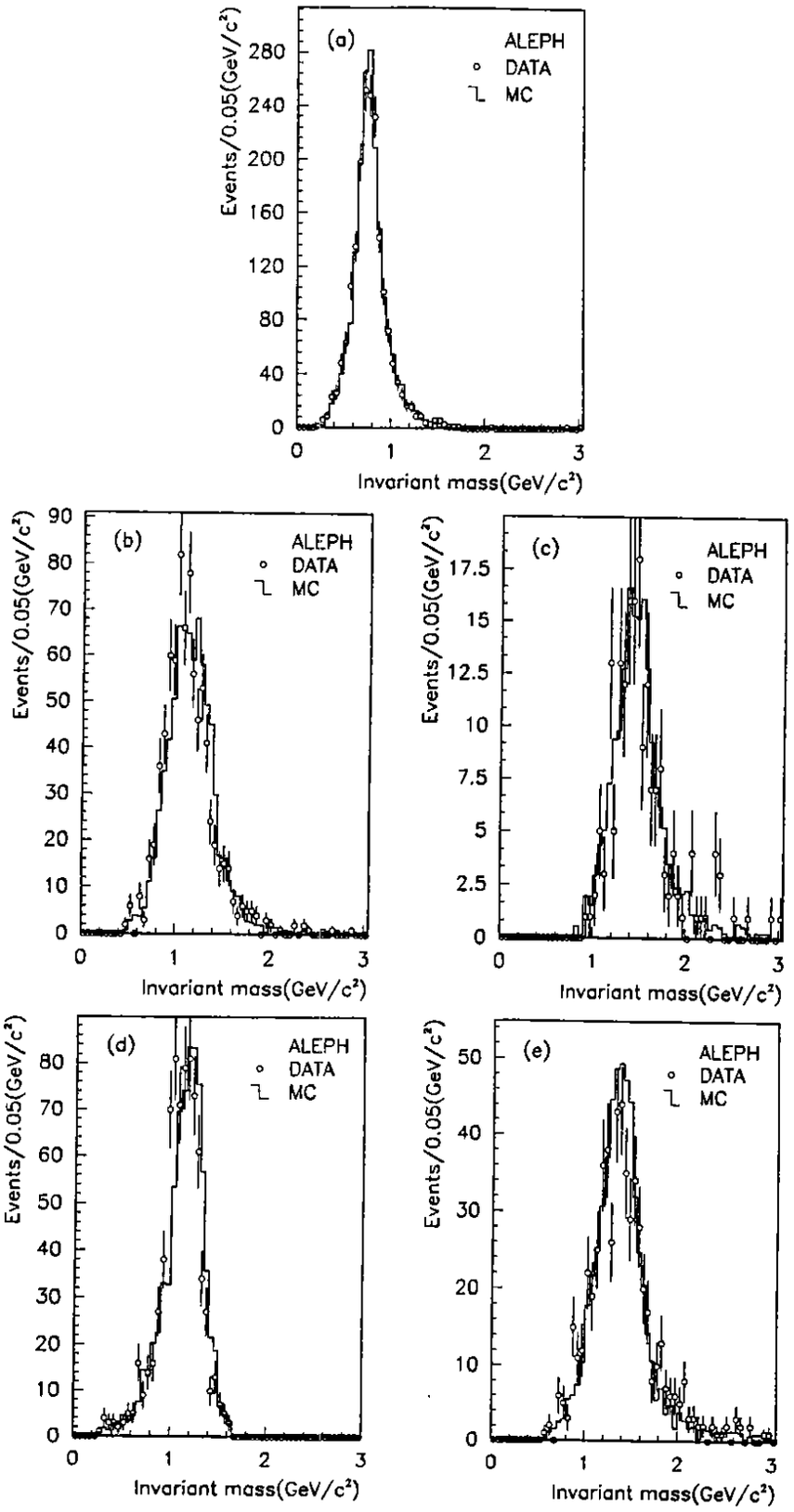

Figure 9: *Distributions (a) – (e) of hadronic invariant mass of all detected final states for classes 4 – 8, respectively. Note that the small excess on the left hand side of the peak in (d) is due to a small contribution of the decays with only two selected tracks(cf. Table 7).*

correlation) is:

$$\sum_{1-\text{prong}} B_i = 85.8 \pm 1.6\ \% \ , \tag{17}$$

and is consistent with the corresponding topological branching ratio (Eq.(12)). This comparison clearly does not constitute a test of the one–prong problem, but rather a consistency check on the systematic effects involved in the analyses.

10 An Exclusive Analysis of Final States With Neutral Pions

The analysis described in the previous section is not based on a completely exclusive definition of the channels with π^0's, since it accepts as π^0 candidates single photons (down to an energy of 250 MeV) not used in a π^0 mass combination. Here, the analysis is restricted to τ decays with fully reconstructed π^0's, so that exclusive channels can be unambiguously defined. Therefore, decays with additional photons are rejected except for the $h3\pi^0$ channel.

Compared to the quasi–exclusive case, the background is expected to be smaller, but the efficiency is much reduced. High energy π^0's are lost: for energies larger than 10 – 15 GeV, it is no longer possible to resolve the two photons. Low energy π^0's are also affected, in particular if they decay asymmetrically into two photons, because of the photon energy thresholds of 250 MeV and 1 GeV (as discussed in section 5). A smaller efficiency also means an increased sensitivity to the dynamics of the hadronic system included in the Monte Carlo generator.

Fig.10 shows the evidence for final states with n π^0's ($n \geq 1$). In all cases, a signal is found with a ratio over background consistent with the Monte Carlo prediction.

The full procedure for the derivation of branching fractions is then repeated using only these fully exclusive channels with π^0's. The results are shown in Table 11 and compared with those from the quasi–exclusive analysis. Good consistency is observed between the two sets and thus there is no evidence for a mode not presently included in the Monte Carlo simulation. Quantitatively, the branching ratios for the modes with π^0's (classes 4, 5, 6, and 8) can be summed (with due attention to correlations):

$$\sum_{\pi^0\text{modes}} B_i^{\text{quasi-exclusive}} = 42.13 \pm 0.63\ \% \ , \tag{18}$$

$$\sum_{\pi^0\text{modes}} B_i^{\text{exclusive}} = 41.91 \pm 1.22\ \% \ , \tag{19}$$

where the quoted uncertainties are only statistical. The difference, taking into account a relative systematic uncertainty due to γ and π^0 reconstruction of 0.8%, provides a measure of possible new modes with photons:

$$B_{\text{new modes}} < 3.4\% \quad \text{at } 95\%\ CL \ . \tag{20}$$

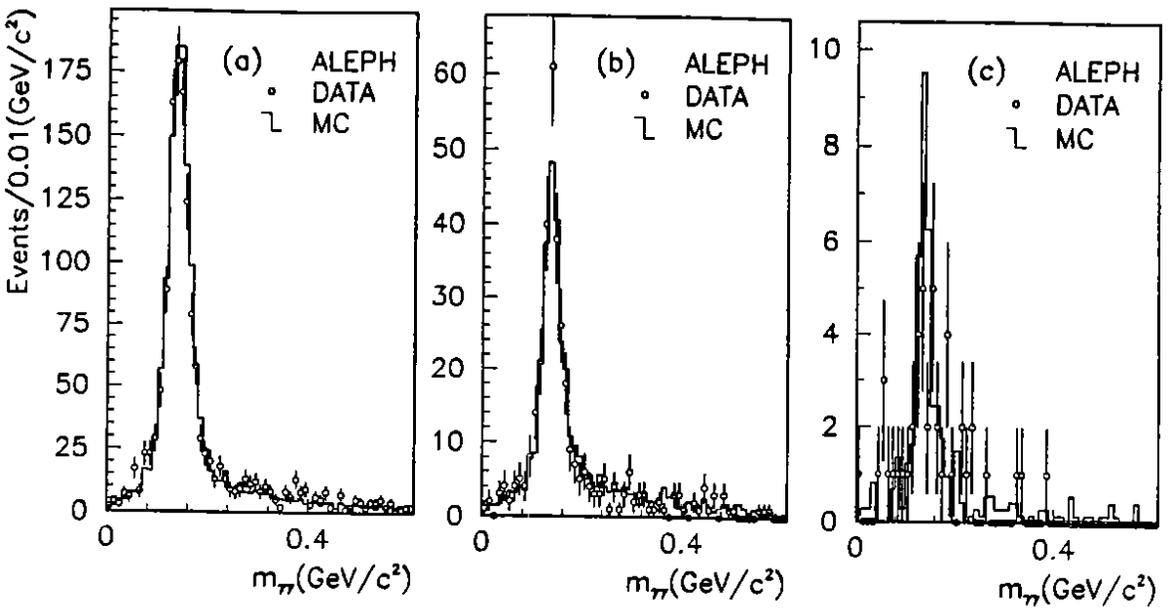

Figure 10: *The invariant mass $m_{\gamma\gamma}$ for decays with (a) two reconstructed photons, (b) four photons with at least one reconstructed π^0, and (c) six or more photons with at least two reconstructed π^0.*

Table 11: *Comparison of the results for the branching ratios B_i of channels with π^0's as obtained from the quasi–exclusive (section 9) and exclusive (section 10) analyses. Also given for each sample are the corresponding efficiency (ε), the other τ channel contamination (f_c) and the number of observed decays. Only statistical errors are given.*

modes	quasi–exclusive			
	ε	f_c	decays	$B_i(\%)$
$h(\pi^0,\gamma)$	0.417	0.112	1849	25.02 ± 0.64
$h(2\pi^0,\pi^0\gamma,2\gamma)$	0.335	0.397	809	10.53 ± 0.66
$h(3\pi^0,2\pi^0\gamma,\pi^0 2\gamma,3\gamma)$	0.273	0.674	186	1.53 ± 0.40
$3h(\pi^0,\gamma)$	0.540	0.265	570	5.05 ± 0.29
modes	**exclusive**			
	ε	f_c	decays	$B_i(\%)$
$h\pi^0$	0.213	0.069	904	25.31 ± 0.87
$h2\pi^0$	0.078	0.147	128	9.09 ± 1.06
$h(3\pi^0 \geq 0\gamma)$	0.025	0.105	10	2.35 ± 0.83
$3h\pi^0$	0.249	0.146	230	5.16 ± 0.41

Therefore, we conclude that the present description of the photonic modes of τ decays in terms of multi–π^0 states is adequate and that the results of the quasi–exclusive analysis are valid. Consequently, the final values quoted for the branching ratios of the different τ decay channels are those from the quasi–exclusive analysis.

11 Discussion

11.1 Comparison with other experiments

Our measurement of topological branching ratios are in good agreement with the world average with a slightly higher three–prong fraction (Fig.11).

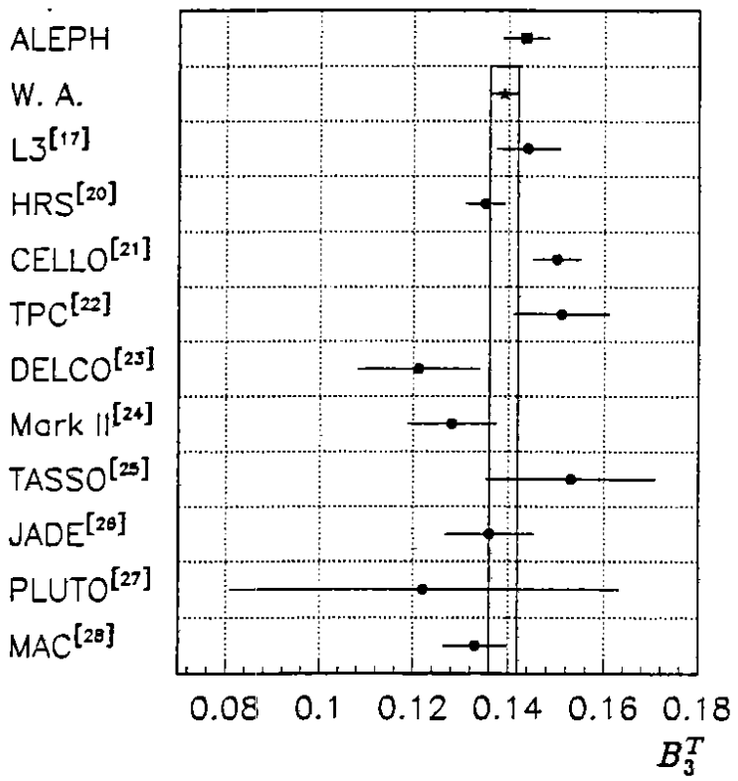

Figure 11: *A comparison of our measured B_3^T with other measurements and their weighted average (W. A., not including our measurement).*

Table 12 gives the comparison between our quasi–exclusive branching ratios and the world–average values[4]. Whenever appropriate, a subtraction is made to account for the small contributions from decay modes included in the defined classes. For instance, to subtract contributions of $K^*\nu_\tau$ from classes 3, 4, and 5 and of $\pi\omega\nu_\tau$ from class 5, a branching ratio value[4] of $(1.4 \pm 0.2)\%$ is used for $K^*\nu_\tau$ and $(1.6 \pm 0.5)\%$ for $\pi\omega\nu_\tau$. For all channels, the world–average values used are those obtained in the full listing of

Table 12: *The comparison of our measured quasi–exclusive branching ratios with the world average[4]. The common relative normalization uncertainty of 1.0% is included in the quoted errors. The values in parentheses are obtained after corrections as described in the text.*

channel	this measurement	world average
$e\overline{\nu}_e$	18.09±0.64	17.9±0.4
$\mu\overline{\nu}_\mu$	17.35±0.55	17.8±0.4
h	13.32±0.55	
$h(K^*$ subtracted)	(12.55±0.55)	11.6±0.6
$h\pi^0$	25.02±1.09	
$\pi\pi^0(K^*$ subtracted)	(24.56±1.09)	22.6±1.1
$h2\pi^0$	10.53±1.05	
$h2\pi^0(K^*$ and $\pi\omega$ subtracted)	(10.23±1.05)	
$\pi2\pi^0$(modes with K subtracted)	(9.85±1.05)	7.5±0.9
$h \geq 3\pi^0$	1.53±0.61	3.0±2.7
$3h$	9.49±0.72	
3π(modes with K subtracted)	(8.93±0.74)	6.7±0.6
$3h \geq 1\pi^0$	4.95±0.71	4.6±1.0
$5\pi \geq 0\pi^0$	0.10±0.05	0.113±0.027

the Particle Data Group[4] from the weighted average of experimental results without additional constraints.

Our measured values for the electron and muon channels are in good agreement with the world average. The values for the channels $h\nu_\tau(\pi\nu_\tau + K\nu_\tau)$ and $\pi\pi^0$ are 1.2σ and 1.3σ above the world average, respectively. A larger disagreement is observed for the a_1 decay mode in both channels: the $h2\pi^0$ and $3h$ modes are 1.7σ and 2.3σ higher than the world average, respectively.

Fig.12 shows the values for B_{3h} and $B_{h2\pi^0}$ from our determinations together with other experiments. A large spread is noticed between the different values.

It should be emphasized that while the world–average values do show a "one–prong problem", they also point to a "three–prong problem" as well: the sum of the average values for the $3h$ and $3h\pi^0$ channels differs from the three–prong topological branching fraction by $(2.6 \pm 1.2)\%$. This inconsistency points towards an underestimation of B_{3h} and/or $B_{3h\pi^0}$.

11.2 Comparison with theory

The measured branching ratios can be compared to the theoretical predictions. The latter are best expressed relative to the electronic branching ratio in order to be insensitive to the theoretically less–known τ width. Reliable predictions based on lepton

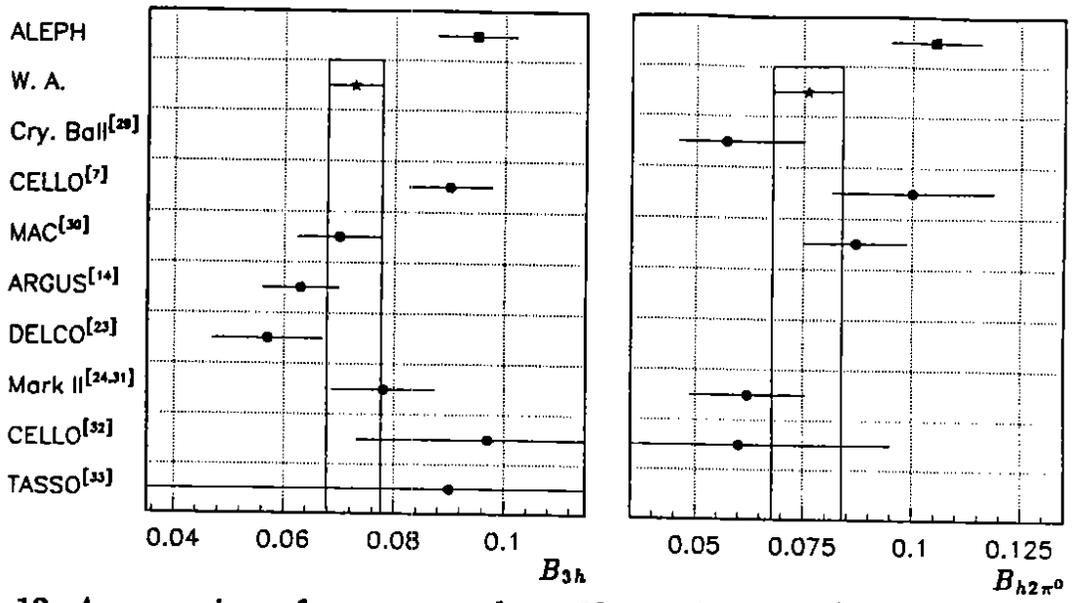

Figure 12: *A comparison of our measured $\tau \to 3h\nu_\tau$ and $\tau \to h2\pi^0\nu_\tau$ branching fractions with the other measurements and their weighted average values (W. A., not including our measurement).*

universality in the charged weak current can be made for the following channels: $\mu\overline{\nu}_\mu\nu_\tau$, $h\nu_\tau$(from $\pi, K \to \mu\overline{\nu}_\mu$), and the multi–pions with G parity= +1 related by CVC to the corresponding e^+e^- annihilation cross sections through an isospin rotation[5,3,6,18]. It should be pointed out that no reliable predictions exist for the G= −1 channels (mostly $\pi 2\pi^0$ and 3π).

Small corrections are applied to the theoretical predictions to account for channels with small branching fractions not included in our Monte Carlo description and distributed among the classes. This is the case for the following channels: $K\pi\pi(1.1\%)$, $K\overline{K}\pi(0.16\%)$, $\eta\pi\pi(0.13\%)$, $K\overline{K}(0.12\%)$, and $\omega\pi$ with $\omega \to \pi^0\gamma(0.24\%)$, where the assumed values come from CVC and e^+e^- data[6] for $\eta\pi\pi$ and $K\overline{K}$, from experiment for $K\overline{K}\pi$[19] and $\omega\pi$[4], and from an estimate based on B_{a_1} and the Cabibbo suppression factor observed in B_K/B_π and B_{K^*}/B_ρ for $K\pi\pi$. These estimates are consistent with experimental values or limits whenever available[4].

The comparison, given in Table 13, shows good agreement between our measured branching ratios and the theoretical predictions for all the channels where the latter can be made reliably.

Finally, the two channels 3π and $\pi 2\pi^0$ are consistent with the dominance of the $a_1 \to \rho\pi$ resonance, since

$$\frac{B_{\pi 2\pi^0}}{B_{3\pi}} = 1.10 \pm 0.14 \,, \tag{21}$$

where a value of one is expected. Further evidence is given by the 2π mass distributions showing a clear ρ signal in both channels, as seen in Fig.13.

Table 13: *The comparison of our measured quasi–exclusive branching ratios with the theoretical predictions.*

ratio	this measurement	theory
$B_{\mu\bar{\nu}_\mu}/B_{e\bar{\nu}_e}$	0.959 ± 0.042	0.973
$B_h/B_{e\bar{\nu}_e}$	0.694 ± 0.037	0.651±0.003
$B_{\pi\pi^0}/B_{e\bar{\nu}_e}$	1.358 ± 0.071	1.33±0.05
$B_{h3\pi^0}/B_{e\bar{\nu}_e}$	0.085 ± 0.034	0.069±0.005
$B_{3h\pi^0}/B_{e\bar{\nu}_e}$	0.274 ± 0.040	0.261±0.019

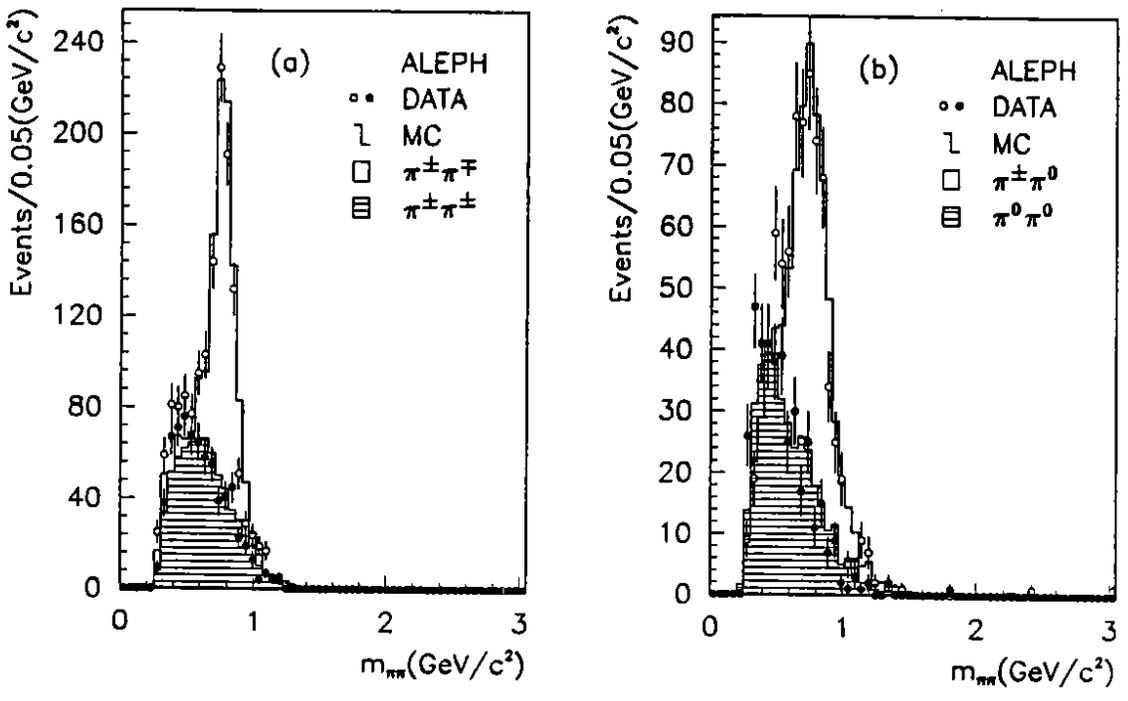

Figure 13: *(a): $m_{\pi^\pm\pi^\mp,\pi^\pm\pi^\pm}$ distributions for the 3π channel; (b): $m_{\pi\pi^0,\pi^0\pi^0}$ distributions for the $\pi 2\pi^0$ channel.*

12 Conclusion

The present analysis on τ branching ratios relies on a large sample of τ decays (8429 for the exclusive branching ratio analysis) provided by Z^0 decays. The selection procedure has both high efficiency (72.4%) and low background contamination (2.4%). Further selection is made to obtain reliable particle identification. Possible systematic effects are checked directly with data.

Topological and exclusive τ branching ratios are measured. In the latter case, events are classified into eight classes, general enough to encompass all possible decay modes. The knowledge of the number of τ's produced from Z^0 decays enables absolute measurements to be made with a small normalization uncertainty (1.0%) under the assumption of lepton universality in Z^0 couplings.

The results show good internal consistency and agree with known theoretical constraints. There is no evidence for undetected decays and these can be limited to 2.1% at 95% CL. It is found that the defined channels are saturated by the expected decay modes. In particular, no significant evidence is observed for sources of photons beyond the expected modes with π^0's and QED radiation with a branching fraction limit of 3.4% at 95% CL. Therefore, these experimental results provide evidence against the previously claimed "one–prong problem".

Channels $\tau \to 3\pi\nu_\tau$ and $\tau \to \pi 2\pi^0\nu_\tau$ are in disagreement with the world average which however was obtained from a wide range of experimental values. The measured ratio between the branching ratios of these two modes is in agreement with the isospin invariance constraint.

13 Acknowledgements

It is a pleasure to thank our colleagues from the SL division for the operation of LEP. We are indebted to the engineers and technicians at CERN and our home institutions for their contributions to ALEPH's success. Those of us from non–member countries thank CERN for its hospitality.

References

[1] A recent detailed review of τ decays could be found in the Proceedings of the Workshop on τ–lepton Physics, Orsay (1990); ed. M. Davier and B. Jean–Marie, Editions Frontières (1991).

[2] T. N. Truong, *Phys. Rev.* **D30** (1984) 1509.

[3] F. J. Gilman and S. H. Rhie, *Phys. Rev.* **D31** (1985) 1066.

[4] Particle Data Group, "Review of Particle Properties", *Phys. Lett.* **239B** (1990) 1.

[5] Yung–Su Tsai, *Phys. Rev.* **D4** (1971) 2821.

[6] S. I. Eidelman and V. N. Ivanchenko, *Phys. Lett.* **257B** (1991) 437.

[7] H. J. Behrend *et al.* (CELLO Coll.), *Z. Phys.* **C46** (1990) 537.

[8] D. Decamp *et al.* (ALEPH Coll.), *Nucl. Instr. Methods* **A294** (1990) 121.

[9] W. B. Atwood *et al.*, CERN–PPE/91–24.

[10] D. Decamp *et al.* (ALEPH Coll.), *Z. Phys.* **C48** (1990) 365.

[11] D. Decamp *et al.* (ALEPH Coll.), *Phys. Lett.* **246B** (1990) 306.

[12] D. Decamp *et al.* (ALEPH Coll.), CERN–PPE/91–105, to be published in *Z. Phys.* **C**.

[13] S. Jadach, B. F. L. Ward, and Z. Was, CERN–TH 5994/91.

[14] S. Jadach, J. H. Kühn, and Z. Was, CERN–TH 5856/90, to appear in *Comp. Phys. Comm.*.

[15] H. Albrecht *et al.* (ARGUS Coll.), *Z. Phys.* **C33** (1986) 7.

[16] S. Jadach, B. van Eijk, and Z. Was, CERN–TH 5857/90, to appear in *Comp. Phys. Comm.*.

[17] B. Adeva *et al.* (L3 Coll.), CERN–L3 031, June 1991.

[18] J. H. Kühn and A. Santamaria, *Z. Phys.* **C48** (1990) 445.

[19] J. J. Eastman, PhD dissertation, LBL–30035, University of California, Berkeley, Dec. 1990.

[20] S. Abachi *et al.* (HRS Coll.), *Phys. Rev.* **D40** (1989) 902.

[21] H. J. Behrend *et al.* (CELLO Coll.), *Phys. Lett.* **B222** (1989) 163.

[22] H. Aihara *et al.* (TPC Coll.), *Phys. Rev.* **D35** (1987) 1553.

[23] W. Ruckstuhl *et al.* (DELCO Coll.), *Phys. Rev. Lett.* **56** (1986) 2132.

[24] W. B. Schmidke *et al.* (Mark II Coll.), *Phys. Rev. Lett.* **57** (1986) 527.

[25] M. Althoff *et al.* (TASSO Coll.), *Z. Phys.* **C26** (1985) 521.

[26] W. Bartel *et al.* (JADE Coll.), *Phys. Lett.* **161B** (1985) 188.

[27] Ch. Berger *et al.* (PLUTO Coll.), *Z. Phys.* **C28** (1985) 1.

[28] E. Fernandez *et al.* (MAC Coll.), *Phys. Rev. Lett.* **54** (1985) 1624.

[29] D. Antreasyan *et al.* (Crystal Ball Coll.), *Phys. Lett.* **259B** (1991) 216.

[30] H. R. Band *et al.* (MAC Coll.), *Phys. Lett.* **B198** (1987) 297.

[31] K. K. Gan *et al.* (Mark II Coll.), *Phys. Rev. Lett.* **59** (1987) 411.

[32] H. J. Behrend *et al.* (CELLO Coll.), *Z. Phys.* **C23** (1984) 103.

[33] R. Brandelik *et al.* (TASSO Coll.), *Phys. Lett.* **92B** (1980) 199.

Imprimé au CERN. Prix: 0.80 Fr.